ACCEPTED VERSION

This is a pre-copyedited, author-produced version of an article accepted for publication in ***Mathematical Medicine and Biology*** *following peer review. The version of record*

J. E. F. Green J. P. Whiteley and J. M. Oliver, H. M. Byrne and S. L. Waters
Pattern formation in multiphase models of chemotactic cell aggregation
Mathematical Medicine and Biology: A Journal of the IMA, 2018; 35(3):319-346

is available online at http://dx.doi.org/10.1093/imammb/dqx005

© The authors 2017. Published by Oxford University Press on behalf of the Institute of Mathematics and its Applications. All rights reserved.

PERMISSIONS

https://academic.oup.com/journals/pages/access_purchase/rights_and_permissions/author_self_archiving_policy

Accepted manuscript
The Accepted Manuscript (AM) is the final draft author manuscript, as accepted for publication by a journal, including modifications based on referees' suggestions, before it has undergone copyediting, typesetting and proof correction. This is sometimes referred to as the post-print version.

Immediately upon publication

- Authors may make their AM available on their non-commercial homepage or blog. They may also privately share their work within their institution for the purposes of research or education, and make copies available to colleagues or students for their personal use providing that the AM is not made publicly available until after the embargo period.
- Authors may also immediately upload their AM to their institutional or other non-commercial subject based repositories (on the proviso that it is not made publicly available until after the specified embargo period)

After embargo

- Authors may upload their AM to an institutional repository or other non-commercial repositories, and make it publicly available. Accepted Manuscripts *may not*> be uploaded or shared on commercial websites or repositories, unless the website or repository has signed an agreement with OUP permitting such uploading or sharing.

Embargo periods may vary between journals. For details of a journal's specific embargo period, please see the information for each individual title in our Accepted Manuscript embargo period list.
When making an accepted manuscript available, authors should include the following acknowledgment as well as a link to the version of record. This will guarantee that the version of record is readily available to those accessing the article from public repositories, and means that the article is more likely to be cited correctly.
This is a pre-copyedited, author-produced version of an article accepted for publication in [insert journal title] *following peer review. The version of record* [insert complete citation information here] *is available online at: xxxxxxx* [insert URL and DOI of the article on the OUP website].

1 June 2020

http://hdl.handle.net/2440/116362

Mathematical Medicine and Biology Page 1 of 29
doi:10.1093/imammb/dqnxxx

Pattern formation in multiphase models of chemotactic cell aggregation

J.E.F. Green[1], *J.P. Whiteley*[2], *J.M. Oliver*[3], *H.M. Byrne*[3] *and S.L. Waters*[3]∗

[1] *School of Mathematical Sciences, University of Adelaide, Adelaide, SA, 5005, Australia.*
[2] *Department of Computer Science, University of Oxford, Oxford, OX1 3QD, UK.*
[3] *Mathematical Institute, University of Oxford, Oxford, OX2 6GG, UK.*

We develop a continuum model for the aggregation of cells cultured in a nutrient-rich medium in a culture well. We consider a two-dimensional geometry, representing a vertical slice through the culture well, and assume that the cell layer depth is small compared with the typical lengthscale of the culture well. We adopt a continuum mechanics approach, treating the cells and culture medium as a two-phase mixture. Specifically, the cells and culture medium are treated as fluids. Additionally, the cell phase can generate forces in response to environmental cues, which include the concentration of a chemoattractant that is produced by the cells within the culture medium. The model leads to a system of coupled nonlinear partial differential equations for the volume fraction and velocity of the cell phase, the culture medium pressure and the chemoattractant concentration, which must be solved subject to appropriate boundary and initial conditions. To gain insight into the system, we consider two model reductions, appropriate when the cell layer depth is thin compared to the typical length scale of the culture well: a (simple) one-dimensional and a (more involved) thin-film extensional flow reduction. By investigating the resulting systems of equations analytically and numerically, we identify conditions under which small amplitude perturbations to a homogeneous steady state (corresponding to a spatially-uniform cell distribution) can lead to a spatially varying steady state (pattern formation). Our analysis reveals that the simpler one-dimensional reduction has the same qualitative features as the thin-film extensional flow reduction in the linear and weakly nonlinear regimes, motivating the use of the simpler one-dimensional modelling approach when a qualitative understanding of the system is required. However, the thin-film extensional flow reduction may be more appropriate when detailed quantitative agreement between modelling prediction and experimental data is desired. Furthermore, full numerical simulations of the two model reductions in regions of parameter space when the system is not close to marginal stability reveal significant differences in the evolution of the volume fraction and velocity of the cell phase, and chemoattractant concentration.

Keywords:
Cell aggregation, Multiphase model, Model reduction, Thin-film extensional flow, Stability analysis

1. Introduction

The movement of many types of cells is influenced by local gradients of diffusible chemicals via a phenomenon known as chemotaxis. Consider, for example, the slime mould *Dictyostelium discoideum*, which usually lives as a single-cell amoeba-like organism in the soil. However, under starvation conditions, the cells produce cyclic-AMP (cAMP) which diffuses through the environment, providing a signal which drives the collective movement of cells up the cAMP gradients that are generated, resulting in cell aggregates called slugs [9]. The bacteria *Escherichia coli* exhibits similar behaviour when cultured *in vitro* under suitable conditions, resulting in the formation of elaborate patterns [2]. Cell

∗Email: waters@maths.ox.ac.uk

© The author 2008. Published by Oxford University Press on behalf of the Institute of Mathematics and its Applications. All rights reserved.

movement via chemotaxis also plays an important role in the progression of diseases such as cancer [22] and Alzheimer's [10, 26], in wound healing [1], and in the growth of tissues both *in vivo* and *in vitro* [6, 12, 14, 23].

Mathematical models of cell aggregation through chemotaxis have a long history, starting with the seminal work of Keller and Segel [18, 19] who considered the formation of multicellular slugs from initially separate cells of *Dictyostelium discoideum*. The Keller-Segel model consists of a pair of coupled reaction-diffusion equations for the evolution of the cell density and chemoattractant concentration. Cell motion is assumed to include two components: unbiased random motion (modelled as a diffusive flux term), and a biased motion up chemical gradients (modelled as a flux term proportional to the chemical concentration gradient), whilst the chemical is assumed to be produced by the cells, to diffuse through the environment, and to undergo natural decay.

The seminal work of [18, 19] underpins many theoretical studies of chemotaxis [15, 35], and many model extensions have been considered (see [4] and references therein). Although the Keller-Segel model may be presented as a phenomenological model, it can also be derived by taking the continuum limit of a biased or reinforced random walk [34, 35]. Of particular relevance to this work is [4], in which an alternative derivation and interpretation of the classical Keller-Segel model employing a multiphase modelling approach is presented. Multiphase models provide a natural framework within which to model biological tissues: these composite materials comprise a variety of interacting constituents, including, for example, different cells types, their associated extra-cellular matrix (ECM), and interstitial fluid. Multiphase models represent the tissue as a mixture of continua, which occupy the same regions of space; the behaviour of the different phases are governed by equations representing mass and momentum conservation. Constitutive relations describe the material properties of the phases and their interactions: the appropriate specification of such constitutive laws allows a variety of biophysical systems to be modelled [29], such approaches having been widely used in tissue engineering [20, 30, 31, 32] and cancer modelling [3, 5].

To understand the pattern-forming potential of both reaction-diffusion and multiphase models, a combination of analytical techniques and numerical solutions has proved useful [11, 25, 27, 29, 33]. Linear analysis can be used to determine the conditions under which spatially uniform (homogeneous) steady states of the model are unstable and, hence, when to expect spatially-structured patterns. Weakly nonlinear analysis can be used to understand the spatial dependence and time evolution of such patterns when the system is close to marginal stability [27, 28, 38]. Combining these insights with numerical simulations yields a more comprehensive description of the system's behaviour than can be obtained through simulation alone.

In this paper, we model cells that proliferate within a culture well, suspended in nutrient-rich medium (referred to subsequently as the cell layer). The cells produce a chemoattractant, which diffuses rapidly in the culture medium, and stimulates the formation of cell aggregates. The model studied here was originally motivated by the formation of aggregates of hepatocytes (a type of liver cell) in tissue engineering [12, 13], but is applicable to many other situations where cells are cultured *in vitro*. We employ a multiphase modelling approach, similar to Byrne and Owen [4], but we additionally include the effects of cell viscosity to account for the resistance to cell motion ~~due, for example, to the presence of the cytoskeletal network inside the cell~~ (as discussed within the multiphase framework by, for example, [24]). In §2 we develop the model and present the full system of governing equations, together with boundary and initial conditions. Insights into the behaviours displayed by the model equations is gained by considering two model reductions, both of which are commonly adopted in the literature [20, 21, 29, 32]. In §3, we consider a one-dimensional (1D) version of the governing equations. In §4, we derive an alternative, thin-film extensional flow model, appropriate when the depth of the cell layer

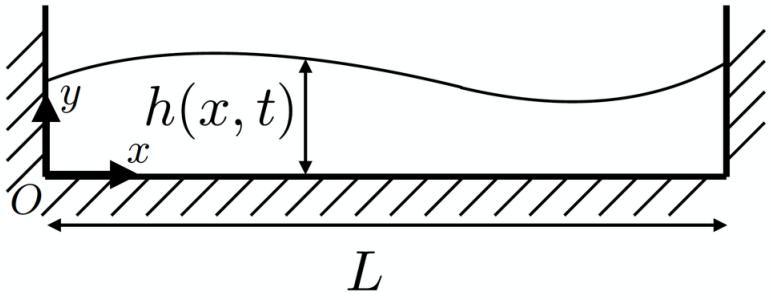

FIG. 1: Schematic showing the model setup in which the cells and culture medium (referred to as the cell layer) occupy a 2D culture well of length L. The height of the cell layer is $h(x,t)$.

is small compared to the lengthscale of the culture well; by considering an asymptotic analysis in this small aspect ratio we obtain a 1D model which, in contrast to the first 1D model, accounts for the effects of cell adhesion to the culture well surface, as well as surface tension at the cell layer-air interface. For both models, we consider the linear stability of the homogeneous steady state to small perturbations. Motivated by the potential for chemotaxis to stimulate cell aggregation, we highlight those features of the system which are stabilising and those which are destabilising. An important result of our study is that while the stabilising effects of interfacial tension and substrate adhesion are captured in the thin-film extensional flow model, only the unstable modes of the system are well captured by the simpler 1D formulation. This has important implications for modelling chemotactic pattern formation, ~~in particular supporting the use of the simpler 1D model~~. We then perform a weakly nonlinear analysis, which yields approximate solutions to the governing equations when the system is close to a marginally stable steady state. We conclude our study with numerical solutions of the 1D reductions in the nonlinear regime, demonstrating intriguing coarsening solutions in the 1D model and the existence of surface-tension-driven oscillations in the thin-film extensional flow model. Finally, in §5, we conclude with a summary of our findings and a discussion of the implications of our results.

2. Governing equations

We adopt a continuum modelling approach in which the cells and nutrient-rich culture medium (referred to subsequently as the cell layer) are treated as a two-phase mixture. We consider a 2D culture domain with Cartesian coordinates $\boldsymbol{x} = (x,y)$ and corresponding coordinate directions $\boldsymbol{i}$, $\boldsymbol{j}$. The culture well occupies the region $0 < x < L$, $y > 0$, while the cell layer occupies the region $0 < x < L, 0 < y < h(x,t)$, where $h(x,t)$ is the height of the cell layer-air interface, and t denotes time (see Figure 1). The volume fractions of the cells and culture medium are denoted by $n(\boldsymbol{x},t)$ and $s(\boldsymbol{x},t)$ respectively, and their velocities are denoted by $\boldsymbol{u}(\boldsymbol{x},t)$ and $\boldsymbol{v}(\boldsymbol{x},t)$. The concentration of the chemoattractant per unit volume of culture medium is given by $c(\boldsymbol{x},t)$, so that sc is the concentration per unit volume of mixture (assuming no voids).

Within the two-phase modelling framework, we account for cell proliferation and death, and the

production of chemoattractant by the cells. Additionally, in the thin-film extensional flow model, since we consider a reduction of the 2D equations appropriate when the cell layer depth is small compared to the length scale of the culture well, we can account for cell-substrate adhesion and surface tension and the cell layer-air interface. Below we summarise our modelling assumptions, and present the governing equations in general form. ~~In §3 and §4 we consider, respectively, a simple 1D version of the equations, and a thin-film extensional flow model obtained in the limit when the depth of the cell and culture medium layer is small compared to its length. Since these two model variants require different boundary conditions, these are presented later, in the relevant sections.~~ As the 1D and thin-film extensional flow models require different boundary conditions, these are presented in the relevant sections (§3 and §4 respectively).

We start by assuming there are no voids, so

$$n+s=1. \tag{2.1}$$

Assuming each phase to be incompressible and of the same density, the conservation of mass equations are given by

$$\frac{\partial n}{\partial t}+\nabla\cdot(n\boldsymbol{u})=J, \tag{2.2a}$$

$$\frac{\partial s}{\partial t}+\nabla\cdot(s\boldsymbol{v})=-J, \tag{2.2b}$$

where J denotes the net rate of mass transfer from culture medium to cells (cells proliferate by absorbing water, and water is liberated when cells die). The force balance for each phase (neglecting inertia) is of the form

$$\nabla\cdot(n\boldsymbol{\sigma}_n)+\boldsymbol{F}_n=\boldsymbol{0}, \tag{2.3a}$$

$$\nabla\cdot(s\boldsymbol{\sigma}_s)-\boldsymbol{F}_n=\boldsymbol{0}, \tag{2.3b}$$

where $\boldsymbol{\sigma}_n$ and $\boldsymbol{\sigma}_s$ are the stress tensors for the cells and culture medium, respectively, and $\boldsymbol{F}_n$ represent the interphase force exerted by the culture medium on the cells.

When specifying the constitutive relations for $\boldsymbol{\sigma}_n$, $\boldsymbol{\sigma}_s$ and $\boldsymbol{F}_n$, we assume that the shear and bulk viscosities of the culture medium are negligible relative to those of the cell phase, and treat the culture medium as an inviscid fluid on the macroscale for which

$$\boldsymbol{\sigma}_s=-p\boldsymbol{I}, \tag{2.4}$$

where p is the fluid pressure and $\boldsymbol{I}$ the identity tensor. The form (2.4) is chosen so that the force balance (2.3b) and the constitutive law prescribed below for the interphase force $\boldsymbol{F}_n$ (see (2.7)) lead to the transport of culture medium being governed by Darcy's law and thus the microscale effects of the culture medium viscosity are included in this sense in the macroscale formulation. We assume that the cell phase can be modelled as a viscous fluid and employ the Newtonian constitutive relation for $\boldsymbol{\sigma}_n$,

$$\boldsymbol{\sigma}_n=-p_n\boldsymbol{I}+\mu\left(\nabla\boldsymbol{u}+(\nabla\boldsymbol{u})^T\right)+\lambda(\nabla\cdot\boldsymbol{u})I, \tag{2.5}$$

where p_n is the cell-phase pressure, T denotes transpose, and μ and λ denote the (effective) shear and bulk cell-phase viscosities, respectively. Cells differ from ordinary viscous fluids, however, in that they can generate forces in response to cues from their environment, such as variations in the local cell phase volume fraction or chemoattractant concentration. We assume these forces manifest themselves in the

form of an additional intraphase pressure [24], which can depend on both the cell phase volume fraction and the chemoattractant concentration, and write

$$p_n = p + \Sigma(n,c), \tag{2.6}$$

where the function $\Sigma(n,c)$ encapsulates the environmental cues described above. Finally, we assume that the culture medium exerts a drag force on the cells, and the drag coefficient is kns, where k is a non-negative constant. Thus there is no drag if either of the two phases is absent. We hence write

$$\boldsymbol{F}_n = -kns(\boldsymbol{u}-\boldsymbol{v}) + p\nabla n, \tag{2.7}$$

noting that the last term in this equation represents the contribution of interfacial forces (see [24] for a detailed derivation).

Substituting (2.4)-(2.7) into (2.3), we obtain the following force balances (using $s = 1-n$)

$$-n\nabla p + \nabla\cdot[\mu n(\nabla\boldsymbol{u} + \nabla\boldsymbol{u}^T)] + \nabla(\lambda n(\nabla\cdot\boldsymbol{u})) - kn(1-n)(\boldsymbol{u}-\boldsymbol{v}) - \nabla\Psi = \boldsymbol{0}, \tag{2.8a}$$

$$-\nabla p - kn(\boldsymbol{v}-\boldsymbol{u}) = \boldsymbol{0}, \tag{2.8b}$$

where, for convenience, $\Psi(n,c) = n\Sigma(n,c)$.

We assume that the chemoattractant diffuses through the culture medium on a timescale much shorter than that associated with the convective transport of the culture medium. We hence neglect advective transport, and make the quasi-steady assumption, leading to the following reaction-diffusion equation

$$D\nabla\cdot[(1-n)\nabla c] + \beta n(1-n) - \alpha(1-n)c = 0, \tag{2.9}$$

where D is the diffusion coefficient. The second term in (2.9) represents chemoattractant production by the cells, and the third term its net rate of decay. The chemoattractant is produced by the cells at a rate β, and released into the culture medium. The production term is thus assumed to be proportional to the product of the volume fractions of the two phases, since there must be contact between them in order for the chemoattractant to enter the culture medium. Natural decay of the chemoattractant occurs at a rate α, and the factor of $1-n$ in the decay term is a result of the volume averaging process (see, for example, [8, 12]).

2.1 *Model simplification*

It is convenient to reduce the number of equations in the model by eliminating $\boldsymbol{v}$ from the system (2.2) and (2.8). Rearranging equation (2.8b) gives

$$\boldsymbol{v} = -\frac{1}{kn}\nabla p + \boldsymbol{u}. \tag{2.10}$$

Substituting (2.10) into the sum of (2.2a) and (2.2b) then yields

$$\nabla\cdot\left(\boldsymbol{u} - \frac{(1-n)}{kn}\nabla p\right) = 0, \tag{2.11}$$

representing global conservation of mass of the mixture. On setting $p_T = p + \Psi$, the system (2.2) and (2.8) reduces to

$$\frac{\partial n}{\partial t} + \nabla\cdot(n\boldsymbol{u}) = J, \tag{2.12a}$$

$$\nabla\cdot\left(\boldsymbol{u}-\frac{(1-n)}{kn}\nabla(p_T-\Psi)\right)=0, \tag{2.12b}$$

$$-\nabla p_T+\nabla\cdot[\mu n(\nabla\boldsymbol{u}+\nabla\boldsymbol{u}^T)]+\nabla(\lambda n\nabla\cdot\boldsymbol{u})=\mathbf{0}. \tag{2.12c}$$

Partial differential equations (2.9) and (2.12) define the evolution of the dependent variables c, n, $\boldsymbol{u}$ and p_T. Equations (2.12a,b) represent mass conservation for the cell phase and mixture respectively, while equation (2.12c) is the force balance for the cell phase.

To close the system, it remains to specify the functions Ψ and J. We assume that

$$\Psi=\frac{\Gamma n}{(1-n)}\exp\left(-\frac{c}{c^*}\right), \tag{2.13}$$

where Γ measures the contractility strength and c^* is a positive constant. This function is phenomenological and models chemotactic movement up gradients in chemoattractant, with a greater effect in areas of lower concentration, which is a behaviour that has been experimentally observed [16]. The dependence on n represents the fact that cells tend to aggregate at low cell densities, but repulsive forces arise due to contact inhibition when n approaches 1. An exponential dependence of the function Ψ on the concentration c was also considered in [4]. For simplicity, we assume in the analysis that follows that J is linear in n (first-order kinetics):

$$J=\kappa(n_s-n), \tag{2.14}$$

where n_s is the equilibrium cell volume fraction and κ is the constant rate of mass transfer.

3. One-dimensional model

We begin by considering a simple 1D reduction of equations (2.9) and (2.12), where cell velocity is denoted by u. Assuming that the cells and culture medium are confined to the region $0<x<L$ (representing the culture well), the model is closed by specifying no flux boundary conditions for cells, culture medium and chemoattractant at $x=0,L$, as follows

$$u=0,\qquad \frac{\partial}{\partial x}(p_T-\Psi)=0,\qquad \frac{\partial c}{\partial x}=0\quad\text{at } x=0,L, \tag{3.1a–c}$$

together with an initial condition for the cell volume fraction. We nondimensionalise as follows, where tildes indicate dimensionless variables, L_a is the length scale of an aggregate, and U is a typical cell velocity scale:

$$x=L_a\tilde{x},\quad u=U\tilde{u},\quad t=\frac{L_a}{U}\tilde{t},\quad p_T=\frac{\mu U}{L_a}\tilde{p}_T,\quad c=\frac{\beta L_a^2}{D}\tilde{c},\quad J=\frac{U}{L_a}\tilde{J}. \tag{3.2}$$

Integrating equation (2.12b) with respect to x, and applying boundary condition (3.1b), gives an expression for $\partial\tilde{p}_T/\partial\tilde{x}$ in terms of $\tilde{u}$. We can then eliminate $\tilde{p}_T$ from the system of equations, so that the dimensionless governing equations become

$$\frac{\partial n}{\partial\tilde{t}}+\frac{\partial}{\partial\tilde{x}}(n\tilde{u}) = \tilde{J}, \tag{3.3a}$$

$$\tilde{M}(n)\tilde{u}-2\frac{\partial}{\partial\tilde{x}}\left(n\frac{\partial\tilde{u}}{\partial\tilde{x}}\right)+\frac{\partial\tilde{\Psi}}{\partial\tilde{x}} = 0, \tag{3.3b}$$

$$\frac{\partial}{\partial\tilde{x}}\left[(1-n)\frac{\partial\tilde{c}}{\partial\tilde{x}}\right]+(1-n)(n-\tilde{\alpha}\tilde{c}) = 0, \tag{3.3c}$$

for $n(\tilde{x},\tilde{t})$, $\tilde{u}(\tilde{x},\tilde{t})$ and $\tilde{c}(\tilde{x},\tilde{t})$ on $0<\tilde{x}<\tilde{L}$, subject to the boundary conditions

$$\tilde{u}=\frac{\partial\tilde{c}}{\partial\tilde{x}}=0 \qquad \text{at } \tilde{x}=0,\tilde{L}, \tag{3.4a,b}$$

where the dimensionless functions and parameters are as follows

$$\tilde{L}=\frac{L}{L_a},\quad \tilde{J}(n)=\tilde{\kappa}(n_s-n),\quad \tilde{M}(n)=\frac{\tilde{k}n}{1-n},\quad \tilde{\Psi}(n,\tilde{c})=\frac{\tilde{\Gamma}n}{1-n}\exp\left(-\frac{\tilde{c}}{\tilde{c}^*}\right), \tag{3.5}$$

$$\tilde{\kappa}=\frac{L_a\kappa}{U},\quad \tilde{k}=\frac{kL_a^2}{(\mu+\lambda/2)},\quad \tilde{\Gamma}=\frac{\Gamma L_a}{(\mu+\lambda/2)U},\quad \tilde{c}^*=\frac{Dc^*}{\beta L_a^2},\quad \tilde{\alpha}=\frac{\alpha L_a^2}{D}. \tag{3.6}$$

Note that setting a value for $\tilde{\kappa}$ (as we do in the analysis that follows) sets the velocity scale U (for a given κ and L_a). In the analysis that follows it is convenient to work in terms of $\tilde{M}(n)$ and $\tilde{\Psi}(n,\tilde{c})$, and we drop tildes for clarity. Note that Byrne and Owen [4] considered the equivalent of equations (3.3) in the limit in which viscosity is neglected (the second term in equation (3.3b)). Here we retain cell phase viscosity to capture the resistance to cell motion ~~due, for example, to the presence of the cytoskeletal network inside the cell.~~

3.1 *Linear stability analysis*

To determine the regimes in which we might expect to observe aggregation, we perform a linear stability analysis. We consider ~~$\alpha=\alpha_0$ and~~ the spatially homogeneous steady state of equations (3.3), given by $n=n_s$, $u=0$ and $c=c_s=n_s/\alpha$ (where the final constraint applies because c_s must satisfy equation (3.3c)). Note that this steady state exists since we have chosen $J(n_s)=0$ (see equation (2.14)). We then introduce small amplitude perturbations of the following form (real part understood)

$$n\sim n_s+\delta\hat{n}e^{iqx+\omega t}+\ldots,\quad u\sim\delta\hat{u}e^{iqx+\omega t}+\ldots,\quad c\sim c_s+\delta\hat{c}e^{iqx+\omega t}+\ldots, \tag{3.7}$$

where q is the wavenumber, ω is the growth rate of the perturbation, $0<\delta\ll 1$, and $\hat{n}$, $\hat{u}$ and $\hat{c}$ are constants. Substituting (3.7) into equations (3.3) and linearising, we find the growth rate ω is

$$\omega=-\kappa-\frac{q^2n_s}{M(n_s)+2q^2n_s}\left(\beta_1+\frac{\beta_2}{\alpha+q^2}\right), \tag{3.8}$$

where

$$\beta_1=\left.\frac{\partial\Psi}{\partial n}\right|_{(n,c)=(n_s,c_s)},\quad \beta_2=\left.\frac{\partial\Psi}{\partial c}\right|_{(n,c)=(n_s,c_s)}. \tag{3.9a,b}$$

Substituting the expressions for Ψ and $M(n)$ from (3.5), we can write the growth rate in terms of k,κ,α,c^*,n_s, $c_s=n_s/\alpha$ and the wavenumber q , as

$$\omega=-\kappa+\frac{\Gamma q^2\exp(-c_s/c^*)}{k+2q^2(1-n_s)}\left(\frac{n_s}{c^*(\alpha+q^2)}-\frac{1}{1-n_s}\right). \tag{3.10}$$

An exemplar plot of the growth rate as a function of wavenumber, given by equation (3.8), is shown in Figure 2a. Note that we have performed the linear stability analysis on an infinite domain, and so have not imposed the boundary conditions (3.4). Imposing the restriction that the domain is of (dimensionless) length 1, say, selects a discrete set of wave numbers corresponding to integer multiples of π

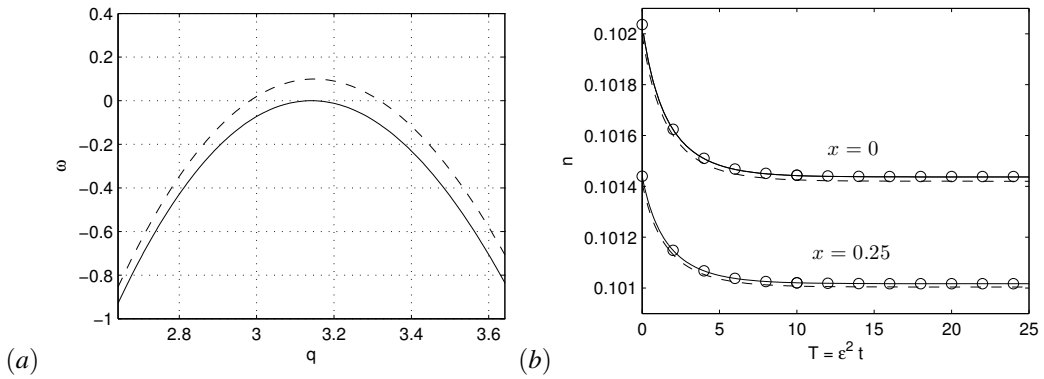

FIG. 2: Parameter values used for both (a) and (b) are $n_1 = 0.1$, $\Gamma = 10^3$, $\kappa = 21.34$, $k = 17.23$ and $c^* = 10^{-3}$. (a) Growth rate, ω, versus wavenumber, q, given by equation (3.8). Solid line: $\alpha = 50$ (the marginal stability case); dashed line: $\alpha = 49.5$. (b) Evolution of $n(0,T)$ and $n(0.25,T)$. Additional parameter values are $L = 1$, $\alpha_0 = 50$, $\alpha_1 = 1$ and $\varepsilon = 0.1$. Solid line: full numerical solution. Dashed line: First-order approximation, $n_s + \varepsilon A(T)$ ($A(T)$ given by equation (3.17)). Circles: Second-order approximation, $n_s + \varepsilon A(T) + \varepsilon^2 A(T)^2 N_2$ (N_2 given by equation (A.7a)).

(to ensure the boundary conditions (3.4) are satisfied). Figure 2a illustrates the effect of varying α for fixed values of the remaining parameters (the exact parameter values are noted in the figure caption). The dashed line corresponds to $\alpha = 49.5$ and we see a band of wavenumbers for which the growth rate is positive, indicating that the homogeneous steady state is linearly unstable to small amplitude perturbations with these wave numbers. We also note the presence of a maximal growth rate, corresponding to the most linearly unstable mode. As the value of α increases, the growth rate decreases for all values of the wavenumber until the maximum growth rate touches zero. This corresponds to the marginal stability case, and in the following section we undertake a weakly nonlinear analysis, which allows us to construct approximate solutions to the governing equations when the system is close to the marginally stable steady state. In particular, such an analysis will reveal the possibility of additional non-spatially uniform steady states for certain choices of parameter values.

To explore the parameter regimes in which we expect to find instability, we calculate q_c, the wavenumber for which ω takes its maximum value by solving $\partial\omega/\partial q = 0$ (where a real solution exists), and use this to calculate $\omega_{max} = \omega(q_c^2)$. In Figures 3 we indicate in white regions of parameter space in which $\omega_{max} > 0$, and where it is possible to observe instability (regions where $\omega_{max} < 0$, so that the system is stable to perturbations of *all* wavenumbers, are shown in black).

In figure 3 we consider the effect on the system stability of varying n_s, corresponding to the equilibrium cell seeding density, and c^* and α, which reflect the sensitivity of the cell generated forces to the chemoattractant and the dimensionless chemoattractant decay rate respectively. We choose to vary these parameters as n_s may be experimentally controlled, and varying c^* and α corresponds to exploring the system dynamics for different cell types. In Figure 3a, we fix α and vary the equilibrium cell seeding density, n_s, and the constant c^* (for small c^*, a small change in c produces a larger change in Ψ than that associated with larger values of c^*). For very small values of n_s, we see that increasing c^* results in the system becoming stable to perturbations of all wavenumbers. However, for larger values of n_s (less that ≈ 0.5) we see the opposite result that increasing c^* results in the system losing stability. In Figure 3b

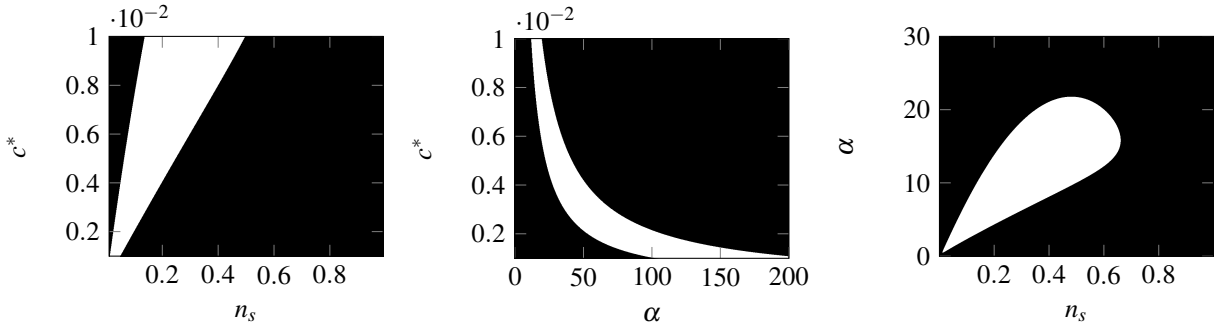

FIG. 3: Stability regions for for $\kappa = k = 1$ and $\Gamma = 100$. White (black) regions indicate parameters values for which instability (stability) is predicted for some (all) wavenumber, q. (a) $\alpha = 10$. (b) $n_s = 0.6$. (c) $c^* = 0.01$.

we instead fix the equilibrium cell seeding density, and vary c^* and α. We observe a region in parameter space where the system may become unstable. Note that the role of α is complicated: increasing α corresponds to the decay rate increasing, which we might expect to be a stabilising effect. However, since $c_s = n_s/\alpha$, increasing α also results in c_s decreasing, which can be destabilising (see equation (3.10)). Finally, in Figure 3c, we fix c^* and vary α and n_s, and we again see a region in parameter space where the system may become unstable. These plots illustrate that the response of a homogenous steady state to small amplitude perturbations depends on the system parameters in a non trivial manner: insights gained from the analysis of the types of mathematical models described here can be used to inform experimental protocols for promoting cell aggregation *in vitro*.

3.2 *Weakly nonlinear analysis*

We start by noting that if we choose a value of $\alpha = \alpha_0$ such that

$$-\kappa = \frac{q^2 n_s}{M(n_s) + 2q^2 n_s}\left(\beta_1 + \frac{\beta_2}{\alpha_0 + q^2}\right), \tag{3.11}$$

then, from equation (3.8), $\omega = 0$, which correspond to the marginal stability case. An asymptotically small reduction to the value of $\alpha = \alpha_0$, ~~which corresponds to the marginal stability case,~~ results in the maximal value of ω becoming small and positive. Thus the growth rate of the perturbations will be asymptotically small, and it is necessary to consider the dynamics of the system on a longer timescale. To satisfy the boundary conditions at $x = 0, 1$ (where here we choose the lengthscale of the culture well to be the aggregate lengthscale), we require $q = m\pi$ (where m is an integer), and we consider here the wavenumber π (again for illustrative purposes). For marginal stability, in addition to $\omega(\pi) = 0$, we also require that the growth rate takes its maximum value at this point, so that $\partial\omega/\partial q = 0$ at $q = \pi$. Differentiating (3.8) with respect to q, we find that for this to be true, we require

$$M(n_s) = \frac{2q^4\beta_2 n_s}{\beta_1(\alpha_0^2 + 2\alpha_0 q^2 + q^4) + \beta_2\alpha_0}, \tag{3.12}$$

which can then be substituted into (3.11) to obtain κ. Conditions (3.11) and (3.12) therefore determine critical parameter values (*e.g.* for $M(n_s)$ ~~, or equivalently k,~~ and κ) for the given wavenumber $q=\pi$. We note that since $M(n_s)=kn_s/(1-n_s)$, from the critical value of $M(n_s)$ we can equivalently determine the critical value for k. The marginal stability case corresponding to $n_s=0.1$, $\alpha=\alpha_0=50$, $\Gamma=10^3$ and $c^*=10^{-3}$ is plotted by the solid line in Figure 2a (for which $k=17.23$ and $\kappa=21.34$).

We now introduce a small parameter, ε, and consider perturbations to α of the form $\alpha=\alpha_0-\varepsilon^2\alpha_1$, and the corresponding long timescale $T=\varepsilon^2 t$. We seek solutions of the form

$$n\sim n_s+\varepsilon n_1+\varepsilon^2 n_2+\cdots,\quad u\sim \varepsilon u_1+\varepsilon^2 u_2+\cdots,\quad c\sim c_s+\varepsilon c_1+\varepsilon^2 c_2+\cdots. \tag{3.13}$$

Details of the weakly nonlinear analysis are presented in Appendix A. Briefly, we substitute (3.13) into equations (3.3) and (3.4) and consider the systems of equations and boundary conditions at successive orders of ε. At $O(\varepsilon)$, we obtain the following expressions for n_1,u_1 and c_1:

$$n_1=A(T)\cos\pi x,\quad u_1=-\frac{\kappa}{n_s\pi}A(T)\sin\pi x,\quad c_1=\frac{A(T)}{\alpha_0+\pi^2}\cos\pi x, \tag{3.14a–c}$$

where the amplitude $A(T)$ is determined at $O(\varepsilon^3)$. At $O(\varepsilon^2)$ we find n_2,u_2 and c_2 to be given by

$$n_2=N_2A^2\cos 2\pi x,\quad u_2=U_2A^2\sin 2\pi x,\quad c_2=C_{21}A^2\cos 2\pi x+C_{22}A^2+C_{23}, \tag{3.15a–c}$$

where N_2, U_2, C_{21}, C_{22} and C_{23} are constant coefficients given in Appendix A. Finally, at $O(\varepsilon^3)$, suppression of the resonant terms (the secularity condition) gives the following equation for $A(T)$:

$$\frac{dA}{dT}=\chi_1A+\chi_2A^3, \tag{3.16}$$

where χ_1 and χ_2 depend on the ~~system parameters~~ governing parameters. We note that the amplitude equation (3.16) is of the canonical form for a pitchfork bifurcation [36], and has at most three fixed points: $A=0$ and $A=\pm\sqrt{(-\chi_1/\chi_2)}$. However, the latter states only exist if χ_1 and χ_2 are of different sign. Depending on the sign of χ_2, equation (3.16) can undergo either a subcritical ($\chi_2>0$) or supercritical ($\chi_2<0$) pitchfork bifurcation.

Equation (3.16) may be solved explicitly, and has solution

$$A(T)=\text{sign}(A(0))\left[\left(\frac{1}{A(0)^2}+\frac{\chi_2}{\chi_1}\right)e^{-2\chi_1T}-\frac{\chi_2}{\chi_1}\right]^{-1/2}. \tag{3.17}$$

The long-time behaviour of this amplitude equation is therefore as follows:

1. For $\chi_1<0$ and $\chi_2>0$, $A\to 0$ if $A(0)<\sqrt{|\chi_1|/\chi_2}$; $A\to\infty$ if $A(0)>\sqrt{|\chi_1|/\chi_2}$;
2. For $\chi_1<0$ and $\chi_2<0$, $A\to 0$;
3. For $\chi_1>0$ and $\chi_2>0$, $A\to\infty$;
4. For $\chi_1>0$ and $\chi_2<0$, $A\to\sqrt{\chi_1/|\chi_2|}$.

We conclude that there are regimes of parameter space for which a small perturbation to the spatially homogeneous marginally stable steady state can lead to spatial patterns on the long time scale (since $A(T)$ multiplies functions of x in equation (3.14) and equation (3.15)). In the next section we provide numerical validation of our weakly nonlinear analysis, before considering the thin-film extensional flow reduction in detail.

3.3 *Numerical solution*

We solve the governing equations and boundary conditions for the one-dimensional model (equations (3.3) and (3.4)) using the finite element method: see, for example, [17]. At each timestep the system of equations are fully coupled, and a backward difference in time is used for stability reasons. A linear approximation is made to the solution on each element, and this approximation is continuous across element boundaries. The resulting non-linear system of algebraic equations is solved using Newton's method [37], with the solution at the previous timestep used as the initial guess. The temporal and spatial resolution is increased until the influence of any further increase in resolution on the solution is not visible on the graphs presented. The code is validated as follows. First, we confirm that the numerical code predicted the same growth rate for small amplitude perturbations to a spatially homogeneous steady state as that predicted by the linear stability analysis. Secondly, by considering the solution behaviour close to marginal stability, we confirm that the numerical results agreed with the predictions of the weakly nonlinear theory (see Figure 5b and 7b below).

To compare the numerical results with the output of the weakly-nonlinear theory, we consider the solution behaviour close to marginal stability: specifically we consider a small perturbation to the value of α corresponding to marginal stability, i.e. we consider $\alpha = \alpha_0 - \varepsilon^2\alpha_1$ where $\alpha_0 = 50$, $\alpha_1 = 1$ and $\varepsilon = 0.1$. We consider an initial condition of the form

$$n = n_s + \varepsilon A(0)\cos qx, \tag{3.18}$$

where $A(0) = 0.02$ and $q = \pi$. We choose the remaining simulation parameters to ensure that condition "4" is met (specific parameter values are reported in caption of Figure 2b). The solid line in Figure 2b shows the dynamics of the system (which we have characterised by plotting $n(0,T)$ and $n(0.25,T)$) obtained numerically), and confirms that the system evolves towards a new steady state. The dashed line shows the evolution of the system predicted by the weakly nonlinear analysis at first order in ε ($n_s + \varepsilon A(T)$). The agreement between the two solutions is excellent. Furthermore, the circles correspond to the predicted evolution of the system given by $n_s + \varepsilon A + \varepsilon^2(A)^2 N_2$. The agreement with the numerical solution is excellent, and the prediction of the weakly nonlinear analysis clearly improves when the $O(\varepsilon^2)$ terms are included. We stress that the agreement between the numerical and analytical solutions holds throughout the computational domain.

As discussed in §3.2, the possibility of additional patterned steady states (predicted by the weakly nonlinear analysis) depends on the choice of χ_1 and χ_2, which in turn depend on the system parameters. We note that α_1 only appears in χ_1, and χ_1 is proportional to α_1: thus changing the sign of α_1 changes the sign of χ_1. We now investigate how transitions between the possible solutions of the system occur as α_1, and hence $\alpha = \alpha_0 - \varepsilon^2\alpha_1$, varies. For $\chi_2 < 0$, the amplitude equation (3.16) is of the canonical form for a supercritical pitchfork bifurcation. For $\chi_1 < 0$, the homogeneous steady state is stable, but as χ_1 increases through zero, the homogeneous solution loses stability to the patterned steady state corresponding to $A = \sqrt{-\chi_1/\chi_2}$. We illustrate this bifurcation in Figure 4a, where, instead of varying χ_1, we vary α, noting that $\alpha = \alpha_0 - \varepsilon^2\alpha_1$, and increasing χ_1 corresponds to increasing α_1 (for our specific choice of parameter values, see caption for details of parameter values). Thus we see that as α decreases, we obtain a patterned steady state: as the chemoattractant signal decays less slowly the formation of cell aggregates is promoted.

For $\chi_2 > 0$, a subcritical pitchfork bifurcation occurs as χ_1 increases through zero. In this parameter regime, increasing α_1 corresponds to *decreasing* χ_1. Hence χ_1 increasing corresponds to α increasing. When $\chi_1 < 0$, the homogeneous steady state is stable, and the patterned state (corresponding to $A = \sqrt{-\chi_1/\chi_2}$) is unstable. As we pass through $\chi_1 = 0$, the homogeneous steady state loses stability as the

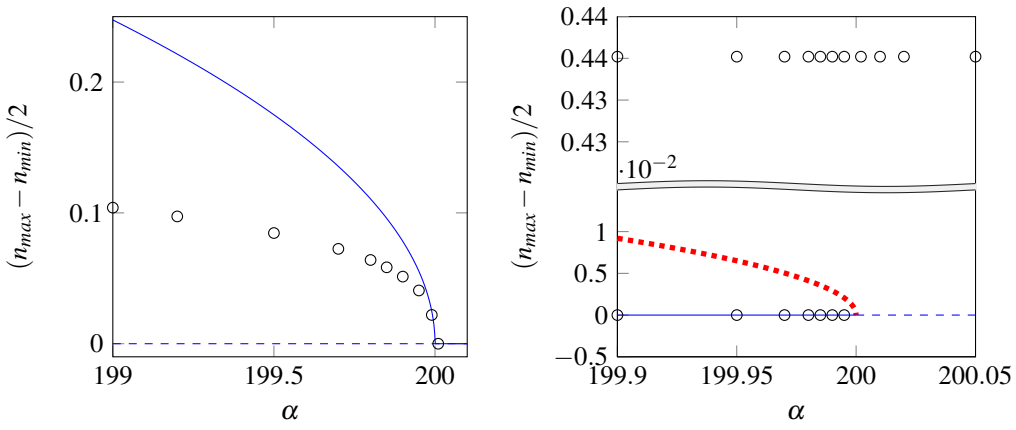

FIG. 4: Parameter values used for both a and b are $\kappa = 1$, $\alpha_0 = 200$, $q = \pi$, $n_s = 0.6$ and $\varepsilon = 0.1$. (a) Bifurcation diagram with additional parameter values: $c^* = 0.001$, $\Gamma = 71.58$ and $k = 4.73$. The solid line is the prediction of the weakly nonlinear theory, the circles are numerical solutions (with $A(0) = 0.02$). The dashed line indicates where the spatially homogeneous steady state is unstable. (b) Bifurcation diagram with additional parameter values: $c^* = 0.0005$, $\Gamma = 109.44$ and $k = 0.72$. The solid (dashed) line shows where the linear stability analysis predicts the spatially uniform steady state to be stable (unstable). The red dotted line shows the unstable patterned steady state, corresponding to $A = \sqrt{|\chi_1|/\chi_2}$. The circles indicate numerical solutions.

patterned state disappears. This bifurcation is illustrated in Figure 4b, where our choice of parameter values is given in the caption. Note that, in this regime, numerical simulations reveal the existence of spatially-patterned fully nonlinear steady states, which persist into the $\chi_1 < 0$ parameter regime.

Thus the onset of aggregation can occur in two qualitatively different ways. In the supercritical case, the pattern amplitude increases gradually as we move further from the bifurcation point, but in the subcritical case the transition from a uniform steady state to a large amplitude pattern occurs much more suddenly.

Finally, we perform numerical simulations of the one-dimensional model in regions of parameter space not close to marginal stability, and where we do not expect to see the system settling down to a steady state close to the spatially homogeneous steady state at long times. In Figure 5 we show the evolution of the cell phase volume fraction, cell velocity and chemoattractant concentration as a function of time. The parameter values are given in the caption of Figure 5. The domain $0 < x < 25$ is discretised into $10,000$ equally sized elements, and at each discretised node x_i the initial conditions are $n(x_i, 0) = 0.1 + 0.001\mathcal{N}(0,1)$ where $\mathcal{N}(0,1)$ is a normal distribution with mean 0 and standard deviation 1. In Figure 5 (a) and 5 (c) we initially see 5 small peaks in the cell phase volume fraction and chemoattractant concentration, while the cell velocity in Figure 5 (b) remains relatively small. As time evolves, these small peaks coarsen into two moderately sized peaks. Our preliminary numerical simulations suggest that this coarsening behaviour is generic. We note that similar coarsening behaviour has been observed elsewhere in two-phase models, see, for example, [7].

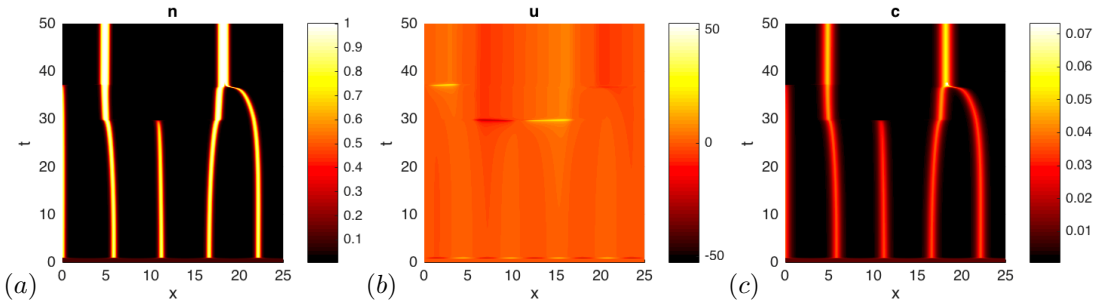

FIG. 5: 1D regime: Evolution of (a) cell phase volume fraction, n, (b) velocity, u, and (c) chemoattractant concentration, c, as a function of time showing behaviour reminiscent of coarsening. The parameters are $\kappa = 0.1$, $k = 1$, $n_s = 0.1$, $\Gamma = 10^3$, $c^* = 5 \times 10^{-3}$, $\alpha = 10$. The domain length considered was $0 < x < 25$, and the simulation was started with initial condition $n(x,0) = 0.1 + 10^{-3}\mathcal{N}(0,1)$, where $\mathcal{N}$ is a normal distribution with mean 0 and standard deviation 1.

4. Thin-film extensional flow model

We now consider the two-dimensional regime in which the cell layer depth is small compared to the lengthscale of the culture well (see Figure 1). After exploiting this small aspect ratio, we will obtain an *extensional* flow model, where the term *extensional* refers to the fact that the leading-order (in the aspect ratio) dependent variables are independent of y. The (dimensional) model equations are now the two-dimensional versions of (2.9) and (2.12), which must be solved subject to suitable boundary conditions, which we now discuss. We start with the boundary conditions for the cell and culture medium phases, before giving boundary conditions for the chemoattractant.

At the side walls of the culture well we assume no flux of cells and culture medium, so that

$$\boldsymbol{i}\cdot\boldsymbol{u} = \boldsymbol{i}\cdot\nabla(p_T - \Psi) = 0 \qquad \text{on } x = 0, L. \tag{4.1a,b}$$

At the base of the culture well, we impose no flux of cells or culture medium as follows

$$\boldsymbol{j}\cdot\boldsymbol{u} = \boldsymbol{j}\cdot\nabla(p_T - \Psi) = 0 \qquad \text{on } y = 0. \tag{4.2a,b}$$

Additionally, we account for adhesion between the cell phase and the base of the culture well via the following slip condition, which relates the horizontal mixture stress to the network velocity

$$\boldsymbol{i}\cdot\left[-p_T\boldsymbol{I} + \mu n(\nabla\boldsymbol{u} + \nabla\boldsymbol{u}^T) + \lambda n(\nabla\cdot\boldsymbol{u})\right]\cdot\boldsymbol{j} = \lambda_s\boldsymbol{u}\cdot\boldsymbol{i} \qquad \text{on } y = 0, \tag{4.3}$$

where λ_s is a measure of the cell-substrate adhesion strength, and the larger λ_s the stronger the adhesion. We note that we have imposed the condition on the mixture stress, but we could also have imposed the condition on the weighted cell phase stress, $n\sigma_n$. This would simply change the first term on the right hand side of equation (4.3), but since this term does not contribute the overall condition remains unchanged. We assume that there is no flux of the cell or culture medium phases through the cell layer-air interface, and impose the following kinematic conditions

$$\boldsymbol{u}\cdot\hat{\boldsymbol{n}} = V_n, \quad \hat{\boldsymbol{n}}\cdot\nabla(p_T - \Psi) = 0, \qquad \text{on } y = h, \tag{4.4a,b}$$

where $\hat{\boldsymbol{n}}$ is the unit outward normal to the surface, and $V_n = h_t/\sqrt{1+h_x^2}$ is the outward normal velocity of the boundary. For simplicity, we also assume that the cell layer-air interface is under constant isotropic tension, γ, and model this via the following interfacial stress boundary condition

$$\left[-p_T\boldsymbol{I} + \mu n(\nabla\boldsymbol{u} + \nabla\boldsymbol{u}^T) + \lambda n(\nabla\cdot\boldsymbol{u})\right]\cdot\hat{\boldsymbol{n}} = -\gamma(\nabla_s\cdot\hat{\boldsymbol{n}})\hat{\boldsymbol{n}}, \tag{4.5}$$

where ∇_s is the surface gradient operator, and $\nabla_s\cdot\hat{\boldsymbol{n}}$ is twice the mean curvature.

We assume that there is no flux of chemoattractant through the walls of the culture well or across the interface $y = h(x,t)$ and, hence (recall that we neglect flux of chemoattractant due to advection), impose

$$\begin{aligned}
\boldsymbol{i}\cdot\nabla c &= 0 \qquad \text{on } x = 0, L, &(4.6a)\\
\boldsymbol{j}\cdot\nabla c &= 0 \qquad \text{on } y = 0, &(4.6b)\\
\hat{\boldsymbol{n}}\cdot\nabla c &= 0 \qquad \text{on } y = h(x,t). &(4.6c)
\end{aligned}$$

In addition to these boundary conditions, initial conditions for n and h must be specified, and these are stated in §4.3 below.

In the analysis that follows we assume that L_a is the lengthscale of an aggregate, and that the typical film thickness is $\hat{\varepsilon}L_a$, where $\hat{\varepsilon} \ll 1$. We non-dimensionalise and rescale as follows

$$x = L\tilde{x}, \quad y = \hat{\varepsilon}L_a\tilde{y}, \quad h = \hat{\varepsilon}L_a\tilde{h}, \quad t = \frac{L_a}{U}\tilde{t}, \quad \boldsymbol{U} = U(\tilde{u}, \hat{\varepsilon}\tilde{v}), \tag{4.7}$$

$$p_T = \frac{\mu U}{L_a}\tilde{p}_T, \quad \Psi = \frac{\mu U}{\hat{\varepsilon}^2 L_a}\tilde{\Psi}, \quad c = \frac{\beta L_a^2}{D}\tilde{c}, \quad J = \frac{U}{L_a}\tilde{J}, \tag{4.8}$$

where U is a typical cell velocity scale. We henceforth omit the tildes from dimensionless variables, and expand the dependent variables in powers of $\hat{\varepsilon}^2$ as follows

$$n \sim n_0 + \hat{\varepsilon}^2 n_1 + \ldots, \tag{4.9}$$

as $\hat{\varepsilon} \to 0$, with similar expansions for u, v, p_T, h and c.

We substitute the above expansions into equations (2.9) and (2.12), together with boundary and interfacial conditions (4.1)-(4.6), and retain the leading-order terms. The x-component of equation (2.12c), together with the conditions (4.3) and the tangential component of (4.5), which states that $\partial u_0/\partial y = 0$ at $y = 0, h_0$, imply that $u_0 = u_0(x,t)$. Similarly, (2.9) together with boundary conditions (4.6b,c), which state that $\partial c_0/\partial y = 0$ at $y = 0, h_0$, implies $c_0 = c_0(x,t)$. Finally, equation (2.12b), together with (4.2b) and (4.4b), give that $n_0 = n_0(x,t)$. Integrating equation (**??**) with respect to y between $y = 0$ and $y = h_0$, using conditions (4.2b) and (4.4a), we derive the following PDE representing cross-layer averaged conservation of mass for the cell phase

$$\frac{\partial}{\partial t}(h_0 n_0) + \frac{\partial}{\partial x}(h_0 n_0 u_0) = J_0 h_0 = \tilde{\kappa} h_0(n_s - n_0), \tag{4.10}$$

where $\tilde{\kappa} = \kappa L_a/U$.

The remaining three equations relating h_0, u_0, n_0 and c_0 are derived by considering the equations at $O(\hat{\varepsilon}^2)$. An expression for p_{T_0} may be found from the y-component of equation (2.12c) together with

the normal component of the interfacial condition (4.5). Substituting this expression for p_{T_0} into the x-component of (2.12c) at $O(\hat{\varepsilon}^2)$, integrating with respect to y between $y=0$ and $y=h_0$ using the conditions (4.2a), (4.3), (4.4a) and the tangential component of (4.5), we obtain the following equation

$$2\frac{\partial}{\partial x}\left(h_0 n_0 \frac{\partial u_0}{\partial x} - n_0 \frac{Dh_0}{Dt}\right) + \Upsilon h_0 \frac{\partial^3 h_0}{\partial x^3} = \Lambda u_0, \tag{4.11}$$

where $\Upsilon = \hat{\varepsilon}\gamma/(\mu U)$, $\Lambda = \lambda_s L_a/(\hat{\varepsilon}\mu)$ and D/Dt is the usual material derivative. Equation (4.11) corresponds to a horizontal cross-layer averaged force balance on the cell layer. We assume that $\Lambda = O(1)$, so that the cell adhesion to the substrate is sufficiently weak that the ensuing flow is extensional at leading order: we note that if Λ is large then anchoring of the cells to the substrate is sufficiently strong that we obtain a parabolic velocity profile for their velocity across the film thickness [21], but we do not pursue this distinguished limit further in this paper.

Integrating equation (2.12b) at $O(\hat{\varepsilon}^2)$ with respect to y between 0 and h_0, using condition (4.2b) and (4.4a) at leading order and (4.2b) and (4.4b) at $O(\hat{\varepsilon}^2)$, gives the following cross-layer averaged equation for mass conservation of the mixture

$$\frac{\partial h_0}{\partial t} + \frac{\partial}{\partial x}(u_0 h_0) = -\frac{\partial}{\partial x}\left(h_0 K(n_0)\frac{\partial \Psi_0}{\partial x}\right), \tag{4.12}$$

where

$$K = \frac{1-n_0}{\tilde{k} n_0}, \quad \Psi_0 = \frac{\tilde{\Gamma} n_0}{(1-n_0)} \exp\left(-\frac{c_0}{\tilde{c}^*}\right), \tag{4.13}$$

and the dimensionless parameters are given by

$$\tilde{k} = \frac{\hat{\varepsilon}^2 k L_a^2}{\mu}, \quad \tilde{c}^* = \frac{c^* D}{\beta L_a^2}, \quad \tilde{\Gamma} = \frac{\hat{\varepsilon}^2 \Gamma L_a}{\mu U}. \tag{4.14}$$

Note that K is the inverse of $M(n)$ introduced in §3. Finally, equation (2.9) at $O(\hat{\varepsilon}^2)$ together with the $O(\hat{\varepsilon}^2)$ versions of (4.2) and (4.6c), gives the cross-layer averaged equation for mass conservation of the chemoattractant

$$\frac{\partial}{\partial x}\left(h_0(1-n))\frac{\partial c_0}{\partial x}\right) + h_0(1-n_0)(n_0 - \tilde{\alpha} c_0) = 0, \tag{4.15}$$

where $\tilde{\alpha} = \alpha L_a^2/D$.

Equations (4.10)-(4.12) and (4.15) are solved subject to the boundary conditions

$$\frac{\partial n_0}{\partial x} = \frac{\partial h_0}{\partial x} = \frac{\partial c_0}{\partial x} = u_0 = 0, \quad \text{at } x = 0, \tilde{L}, \tag{4.16a–c}$$

where $\tilde{L} = L/L_a$ and initial conditions must be specified for n_0 and h_0. In contrast to the 1D model considered in §3 we now have an additional equation for the film height, h_0. Moreover, this model reduction retains the effects of both surface tension and cell-substrate adhesion at leading order. A similar set of governing equations were derived in [21] to describe cell motility: [21] also describes the relationship with the single-phase Trouton model. We note that in the limit $\Upsilon \to \infty$, with all other parameters held fixed, the force balance (4.11), together with the boundary conditions (4.16a–cb) and global conservation of mass, imply that h_0 is a constant; taking h_0 to be constant in governing equations

(4.10) and (4.12) and applying the boundary conditions (4.16a–ca,d), implies that the evolution of n_0 and c_0 are governed by the diffusion equation

$$\frac{\partial n_0}{\partial t} = \frac{\partial}{\partial x}\left(n_0 K(n_0)\frac{\partial \Psi_0}{\partial x}\right) + \tilde{\kappa}(n_s - n_0), \tag{4.17}$$

together with equation (4.15). This reduced system (corresponding to $\Upsilon \to \infty$) is identical to that derived in [4] from a 1D version of the model when viscous effects are neglected. As such, it is the same as the 1D model (3.3) when the viscous term in (3.3b) is ignored.

In the remainder of the paper, we omit the tildes and zero subscripts for clarity. We now proceed to perform both linear and weakly nonlinear analyses for these thin-film equations analogous to §3.

4.1 *Linear stability analysis*

As before, we identify regimes in which aggregation might occur by performing a linear stability analysis. ~~For $\alpha = \alpha_0$ we obtain~~ We consider a homogeneous steady state of equations (4.10)-(4.12) and (4.15), given by $n = n_s$, $h = h_s$, $u = 0$ and $c = c_s = n_s/\alpha$ (where the final constraint applies because c_s must satisfy equation (4.15)). We then introduce small amplitude perturbations of the following form (real part understood)

$$n \sim n_s + \delta\hat{n}e^{iqx+\omega t} + \ldots, \quad h \sim h_s + \delta\hat{h}e^{iqx+\omega t} + \ldots, \quad u \sim \delta\hat{u}e^{iqx+\omega t} + \ldots, \quad c \sim c_s + \delta\hat{c}e^{iqx+\omega t} + \ldots, \tag{4.18}$$

where q is the wavenumber, ω is the growth rate of the perturbation, $0 < \delta \ll 1$ and $\hat{n}$, $\hat{h}$ $\hat{u}$, $\hat{c}$ are constants. Substituting (4.18) into equations (4.10)-(4.15) and linearising, we obtain the following relations

$$\begin{aligned}
\omega h_s\hat{n} + \omega n_s\hat{h} + iqn_s h_s\hat{u} &= -\kappa h_s\hat{n}, && \text{(4.19a)}\\
-2q^2 h_s n_s\hat{u}_n - 2iq\omega n_s\hat{h} - iq^3 h_s\Upsilon\hat{h} - \Lambda\hat{u} &= 0, && \text{(4.19b)}\\
\omega\hat{h} + iqh_s\hat{u} &= q^2 h_s K(n_s)(\beta_1\hat{n} + \beta_2\hat{c}), && \text{(4.19c)}\\
\hat{n} - (\alpha + q^2)\hat{c} &= 0, && \text{(4.19d)}
\end{aligned}$$

where β_1 and β_2 are defined in equation (3.9). The growth rate is then given by

$$\left[\omega + \kappa + q^2 n_s K(n_s)\left(\beta_1 + \frac{\beta_2}{\alpha + q^2}\right)\right]\left[\omega(\Lambda + 4q^2 n_s h_s) + q^4 h_s^2\Upsilon\right] = 0. \tag{4.20}$$

Equation (4.20) holds if either of the expressions in square brackets is zero. Setting the expression in the second bracket to zero we obtain a negative value of ω, which corresponds to stable perturbations to the base state. Thus the effects of interfacial surface tension and substrate adhesion, which are retained in this model and captured by the terms involving Υ and Λ respectively, are stabilising. By setting the expression in the first bracket to zero, it is possible to determine parameter values for which the growth rate for a prescribed wave number is positive, indicating regions of instability. Since $q^2 n_s K(n_s) > 0$, a necessary condition for instability to occur (recalling that $\beta_2 < 0$) is that

$$\beta_1 + \frac{\beta_2}{\alpha} < 0. \tag{4.21}$$

We also require $\beta_1 > 0$ to avoid ill-posedness (to ensure arbitrarily small wavelength perturbations (corresponding to $q \to \infty$) have finite growth rate).

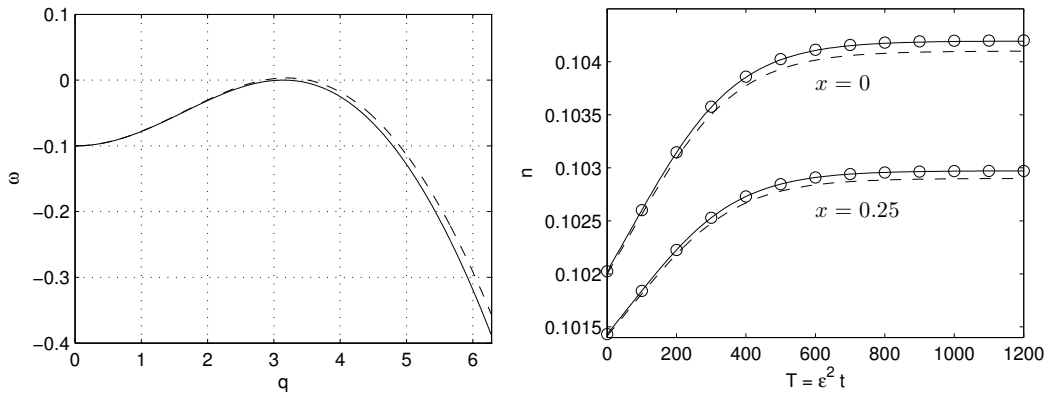

(a) (b)

FIG. 6: Common parameter values for (a) and (b) are $n_s = 0.1$, $h_s = 1$, $\Gamma = 10^3$, $\Lambda = 0.1$, $\Upsilon = 1$, $\kappa = 0.1$, $k = 5069.37$ and $c^* = 1.7 \times 10^{-3}$. (a) Dispersion relation, given by equation (4.20). Solid line: $\alpha = 30$ (the marginal stability case); dashed line: $\alpha = 29$. (b) Evolution of $n(0,T)$ and $n(0.25,T)$. Additional parameter values are $L = 1$, $\alpha_0 = 30$, $\alpha_1 = 1$, $\varepsilon = 0.1$ and A(0)=0.02. Solid line: full numerical solution; dashed line: first-order solution $n_s + \varepsilon A(T)$; Circles: second-order solution $n_s + \varepsilon A(T) + \varepsilon^2(N_{21} + N_{22})A(T)^2$ (N_{21} and N_{22} given by equations (B.8a) and (B.8b) respectively).

If $\beta_1 > 0$ and condition (4.21) is satisfied, the range of unstable wavenumbers must be finite (since the β_2 term vanishes as $q \to \infty$). Hence, we can determine the wavenumbers q_c with the highest growth rates as being the roots of $\partial\omega/\partial q = 0$, which gives

$$q_c^2 = -\alpha \pm \sqrt{\frac{-\alpha\beta_2}{\beta_1}}. \tag{4.22}$$

Note that the positive root of equation (4.22) corresponds to $q_c^2 > 0$ provided the instability criterion (4.21) is fulfilled. A typical dispersion relation is plotted in Figure 6a, where the effect of varying α for fixed values of the remaining parameters (see figure caption for parameter values) can be seen. The dashed line corresponds to $\alpha = 29$, and the solid line to $\alpha = 30$ (the marginal stability case). As in §3.1, we have performed the linear stability analysis on an infinite domain and note that restricting the domain size again constrains the wavenumbers which can be selected.

We comment also that exploring the parameter regimes in which we expect to find instability reveals similar stability regime plots to those for the one-dimensional model and depicted in Figure 3. This is unsurprising given the similarity of the expressions for the growth rate for the one-dimensional and thin-film extensional cases, given by (3.8) and the term in the first square bracket of equation (4.20), respectively.

4.2 *Weakly nonlinear analysis*

We now repeat the weakly nonlinear analysis presented in §3.2 for this extensional flow case, and omit many of the details for brevity. We again consider the wavenumber $q = \pi$, and select parameter values

for which the maximal growth rate is zero, corresponding to $\alpha = \alpha_0$ (see the caption of Figure 6a for details). As before, we consider perturbations to α of the form $\alpha = \alpha_0 - \varepsilon^2\alpha_1$. In summary, we seek solutions of the form

$$n \sim n_s + \varepsilon n_1 + \varepsilon^2 n_2 + \cdots,\ u \sim \varepsilon u_1 + \varepsilon^2 u_s + \cdots,\ c \sim c_s + \varepsilon c_1 + \varepsilon^2 c_s,\ h \sim h_s + \varepsilon h_1 + \varepsilon^2 h_s + \cdots \quad (4.23)$$

as $\varepsilon \to 0$ wherein

$$n_1 = A(T)\cos\pi x, \quad u_1 = \mathscr{U}A(T)\sin\pi x, \quad c_1 = \mathscr{C}A(T)\cos\pi x, \quad h_1 = \mathscr{H}A(T)\cos\pi x, \quad (4.24)$$

and

$$n_2 = N_{21}A^2\cos 2\pi x + N_{22}A^2, \quad u_2 = U_2A^2\sin 2\pi x, \quad (4.25a)$$

$$h_2 = H_2A^2\cos 2\pi x, \quad c_2 = C_{21}A^2\cos 2\pi x + C_{22}A^2 + C_{23}. \quad (4.25b)$$

We find that $\mathscr{U}$, $\mathscr{C}$, and $\mathscr{H}$ are given by

$$\mathscr{U} = -\frac{\kappa}{n_s\pi}, \quad \mathscr{C} = \frac{1}{\alpha_0 + \pi^2}, \quad \mathscr{H} = -\frac{\kappa}{\Upsilon h_s\pi^4}(\Lambda + 2h_s\pi^2), \quad (4.26)$$

and N_{21}, N_{22}, U_2, H_2, C_{21}, C_{22} and C_{23} are constants, whose values are specified in Appendix B. The amplitude, $A(T)$, satisfies an equation of the form given in equation (3.16) and regions of parameter space can be identified in which A approaches a non-zero constant value for long times.

4.3 *Numerical solution*

We solve equations (4.10)-(4.12) and (4.15) subject to the boundary conditions (4.16a–c) for the thin-film extensional flow model, by first recasting them in terms of the integrated-mass variable

$$m(x,t) = \int_0^x h(s,t)\,ds. \quad (4.27)$$

Using the boundary conditions on u, n and c at $x = 0$ in (4.16a–c), equation (4.12) can be rewritten in the form

$$u = -\frac{\partial m}{\partial t}\left(\frac{\partial m}{\partial x}\right)^{-1} - K(n)\frac{\partial \Psi}{\partial x}, \quad (4.28)$$

revealing that both h and u may be eliminated from the governing equations in favour of m, as we shall now describe. Subtracting n times equation (4.12) from equation (4.10) implies that the evolution of n is governed by the nonlinear second-order reaction-advection-diffusion equation

$$\frac{\mathrm{D}n}{\mathrm{D}t} = n\left(\frac{\partial m}{\partial x}\right)^{-1}\frac{\partial}{\partial x}\left(K(n)\frac{\partial m}{\partial x}\frac{\partial \Psi}{\partial x}\right) + J(n), \quad (4.29)$$

where the material derivative may be written in terms of m, n and c using (4.28). Similarly (4.11) implies that the evolution of m is governed by the nonlinear fourth-order diffusion equation

$$\frac{\partial m}{\partial t} + \frac{\Gamma}{\Lambda}\left(\frac{\partial m}{\partial x}\right)^2\frac{\partial^4 m}{\partial x^4} = \frac{2}{\Gamma}\frac{\partial m}{\partial x}\frac{\partial}{\partial x}\left(n\frac{\partial m}{\partial x}\frac{\partial u}{\partial x} - n\frac{\mathrm{D}}{\mathrm{D}t}\left(\frac{\partial m}{\partial x}\right)\right) - K(n)\frac{\partial m}{\partial x}\frac{\partial \Psi}{\partial x}, \quad (4.30)$$

where u is given by (4.28); we emphasise that the terms on the right-hand side of (4.30) contain mixed partial derivatives of m of lower order than the fourth-order term on the left-hand side. By writing

$$r = -\frac{\partial^2 m}{\partial x^2}, \tag{4.31}$$

we may write equation (4.30) as

$$\frac{\partial m}{\partial t} - \frac{\Gamma}{\Lambda}\left(\frac{\partial m}{\partial x}\right)^2 \frac{\partial^2 r}{\partial x^2} = \frac{2}{\Gamma}\frac{\partial m}{\partial x}\frac{\partial}{\partial x}\left(n\frac{\partial m}{\partial x}\frac{\partial u}{\partial x} - n\frac{\mathrm{D}}{\mathrm{D}t}\left(\frac{\partial m}{\partial x}\right)\right) - K(n)\frac{\partial m}{\partial x}\frac{\partial \Psi}{\partial x}, \tag{4.32}$$

Finally, we note that the evolution of c is governed by (4.15) with $h = \partial m/\partial x$.

Equations (4.15), (4.29), (4.31) and (4.32) are then a system of second-order equations in space (for c, n, m and r), which are solved subject to boundary conditions (by (4.16a–c))

$$\frac{\partial c}{\partial x} = \frac{\partial n}{\partial x} = \frac{\partial m}{\partial x} = r = 0, \quad \text{at } x = 0,\, 1, \tag{4.33a–c}$$

and initial conditions which must be specified for n and m. These equations are solved numerically using the finite element method, see §3.3 for details.

In Figure 6b, we compare numerical simulations of equations (4.10)-(4.12) and (4.15) subject to boundary conditions (4.16a–c) and initial conditions

$$n(x,0) = n_s + \varepsilon A(0)\cos(\pi x), \quad h(x,0) = 1 - 0.0213A(0)\varepsilon\cos(\pi x), \tag{4.34}$$

with the predictions of the weakly nonlinear analysis. The solid line shows the evolution of $n(0,T)$ and $n(0.25,T)$ given by the numerical solution of the governing equations, while the dashed line corresponds to the prediction of the weakly nonlinear analysis, accurate to first order, and the circles correspond to the second-order accurate prediction (which again is almost indistinguishable from the full numerical solution). Again, excellent agreement can be seen between the numerical and asymptotic predictions, and this agreement holds for all values of x. The bifurcation structure of the extensional flow case is qualitatively similar to the 1D case, with the weakly nonlinear analysis revealing that both subcritical and supercritical pitchfork bifurcations are possible, depending on the choice of parameter values. Thus, for brevity, we do not present bifurcation diagrams for this regime.

Finally, we perform numerical simulations of the thin-film extensional flow model in regions of parameter space not close to marginal stability, and where we do not expect to see the system settling down to a steady state close to the spatially homogeneous steady state at long times. In Figure 7 we show the evolution of the cell phase volume fraction, cell velocity, chemoattractant concentration, and film height. The domain $0 < x < 10$ is discretised into 10,000 equally sized elements, and at each node x_i the initial conditions are $n(x_i,0) = n_s + 10^(-3)\mathcal{N}(0,1)$, $h(x_i,0) = h_s$ where $\mathcal{N}(0,1)$ is the normal mode distribution with mean 0 and standard deviation 1, as before. Parameter values are given in the caption of Figure 7. In contrast to Figure 5 and as illustrated by analogous plots in Figure 7, our preliminary numerical simulations of the thin-film extensional flow model suggest that an initial pattern does not coarsen on a moderate timescale, though the effects of capillarity are readily observed in the form of surface-tension-driven oscillations that eventually decay.

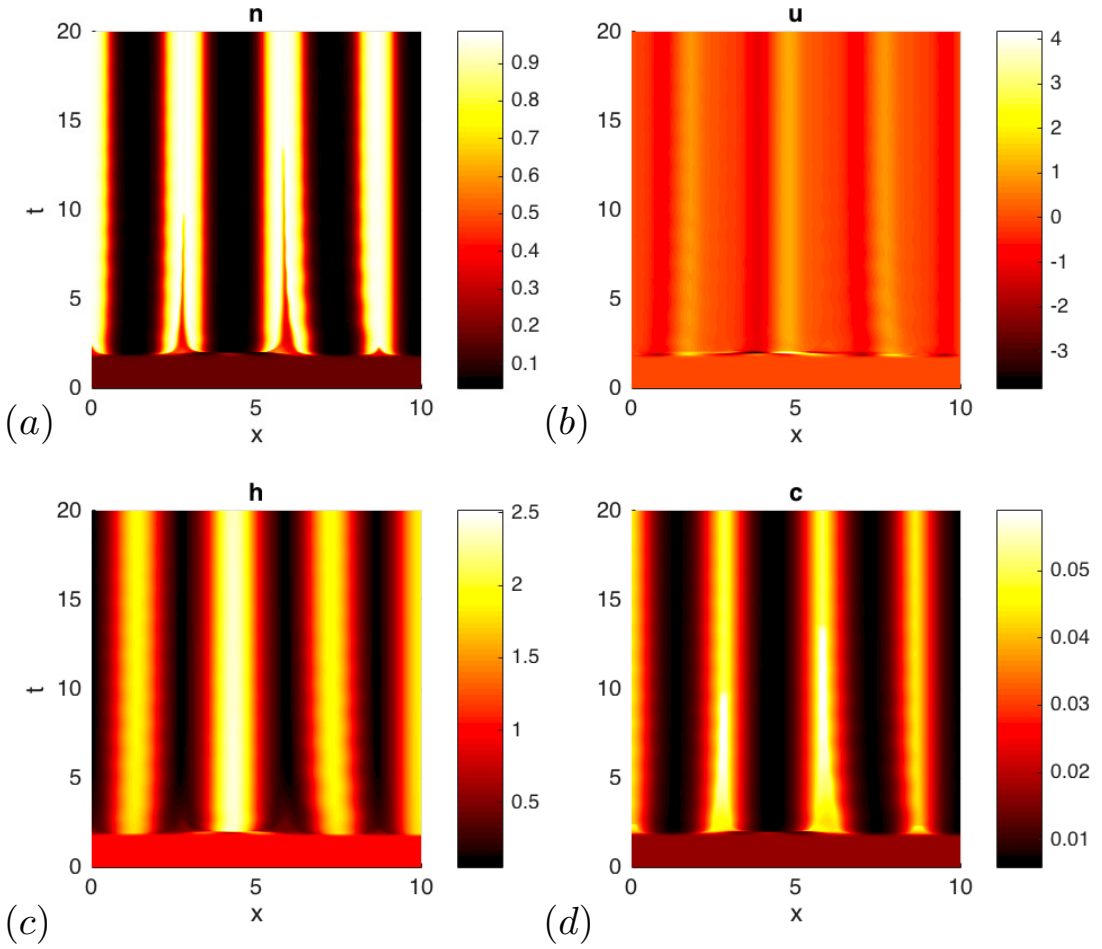

FIG. 7: Extensional regime: Evolution of (a) the cell phase volume fraction, n, (b) velocity, u, (c) the chemoattractant concentration, c, and (d) film height h, as a function of time. The parameter values are $n_s = 0.17$, $h_s = 1$, $c^* = 5 \times 10^{-3}$, $\alpha = 10$, $\Lambda = 1$, $\Gamma = 100$, $\Upsilon = 0.1$, $k = 1$, $\kappa = 1$. The domain length is $0 < x < 10$ and the initial conditions are $n(x,0) = 0.17 + 10^{-3}\mathcal{N}(0,1)$ (where $\mathcal{N}(0,1)$ is a normal distribution with mean 0 and standard deviation 1) and $h = 1$.

5. Discussion and Conclusions

We employed two-phase mixture theory to model the aggregation of cells cultured in nutrient-rich medium in a culture well. The equations are developed by imposing mass and force balances for each phase and, through the specification of appropriate constitutive laws, we have been able to account for key physical processes associated with chemotactic cell aggregation. In this application, the flow of culture medium is governed by Darcy's law, and the cell phase is modelled as a viscous fluid, which additionally can generate forces in response to environmental cues, *e.g.* variations in local cell phase volume fraction and chemoattractant concentration. The cells produce and respond to a chemoattractant, which

both diffuses and decays within the culture medium. Additionally, we account for cell proliferation and death, surface tension at the cell layer-air interface, cell-substrate adhesion, and drag between the two phases. We note that alternative constitutive laws could be specified within this modelling framework to reflect alternative dominant physical processes.

We considered two reductions of the two-dimensional systems of coupled nonlinear partial differential equations: a (simple) one-dimensional reduction and a (more-involved) thin-film extensional flow reduction, exploiting the observation that the cell layer depth is thin compared to the typical length scale of the culture well. In both scenarios, we analysed the response of a spatially-uniform homogeneous steady state to small amplitude perturbations. ~~We first considered the linear stability of the homogeneous steady state to such perturbations, demonstrating that in certain parameter regimes the homogeneous steady state is linearly unstable.~~ Two key results of the paper are the relationship between the growth rate ω and the wavelength q of the linear perturbation to the spatially homogeneous steady state (given by equation (3.10) in the 1D model and (4.20) in the thin-film extensional flow model). We demonstrated that in certain parameter regimes the homogeneous steady state is linearly unstable. In both cases, we noted the presence of a maximal growth rate, corresponding to the most linearly unstable mode. We then identified parameter values for which this maximal growth rate was zero, corresponding to the marginal stability case and performed weakly nonlinear analyses to determine system dynamics close to the marginally stable steady state. An additional result in the derivation of the amplitude equation for $A(T)$ given by equation (3.16). By analysing the long-time behaviour of this equation we identified parameter regimes that give rise to non-spatially uniform steady states.

This detailed analysis motivates the use of the simple 1D reduction when insights into the qualitative behaviour of the system is sought. However, if detailed quantitative agreement between modelling prediction and experimental data is required, it may be desirable to use the thin-film extensional flow reduction. While we have shown that two different model reduction approaches to obtaining 1D equations give qualitatively similar behaviours in the linear and weakly nonlinear regimes, the question remains as to whether differences may be observed in the fully nonlinear regimes. To explore this, we performed numerical simulations of the respective 1D reductions in regions of parameter space not close to marginal stability, and where we did not expect to see the system settling down to a steady state close to the spatially homogeneous steady state at long times. In the 1D case we demonstrated the possibility of coarsening behaviour. In contrast, preliminary numerical simulations of the thin-film extensional flow model suggested that coarsening is not observed on a moderate timescale, though the effects of capillarity are readily observed in the form of surface-tension-driven oscillations that eventually decay.

~~In Figure~~ 5 ~~we show the evolution of the cell phase volume fraction, cell velocity and chemoattractant concentration as a function of time for the 1D reduction. In Figure~~ 5 ~~(a)(i) and~~ 5 ~~(c)(i) we initially see 10 small peaks in the cell phase volume fraction and chemoattractant concentration, while the cell velocity in Figure~~ 5 ~~(b)(i) remains relatively small. As time evolves, these small peaks coarsen, firstly into four moderately sized peaks and eventually into two large peaks. While the transition from 10 small peaks to 4 intermediate sized peaks is relatively rapid, as illustrated by the finer-scale plots in Figures 5(a)(ii)–(c)(ii), the transition from 4 to 2 peaks is much more gradual and occurs through two of the intermediate peaks merging and one of them decaying. Our preliminary numerical simulations suggest that this coarsening behaviour is generic. In contrast and as illustrated by analogous plots in Figure~~ 7, ~~our preliminary numerical simulations of the thin-film extensional flow model suggest that an initial pattern does not coarsen on a moderate timescale, though the effects of capillarity are readily observed in the form of surface-tension-driven oscillations that eventually decay.~~

In this paper, we have analysed in detail the pattern-forming potential of two reduced multiphase models for chemotactic cell aggregation. Our approach reveals that these reductions share many of the

same qualitative features, hence motivating the use of the simpler 1D reduction. The model framework is sufficiently flexible that additional biophysical effects could be incorporated and a similar analysis would enable choices as to which model reduction is more applicable to be justified.

6. Acknowledgements

JEFG acknowledges an Australian Research Council Discovery Early Career Researcher Award (DE130100031).

A. One-dimensional model

The one-dimensional problem is governed by equations (3.3) subject to boundary conditions (3.4). Details of the analysis are given in §3.2 , and we briefly recap the approach here. We undertake a weakly-nonlinear analysis (when the dimensionless domain length is 1) to construct approximate solutions to the governing equations when the system is close to the marginally stable steady state. We consider perturbations to the spatially homogeneous steady state $n = n_s,\ u = 0,\ c = c_s$ with wavenumber $q = \pi$. A set of parameter values $\alpha = \alpha_0, \Gamma, c^*, k, \kappa$ is chosen so that the growth rate is zero at $q = \pi$ and is also maximal there. We then consider perturbations to α of the form $\alpha = \alpha_0 - \varepsilon^2\alpha_1$, and seek solutions of the form (3.13). We proceed by considering the system of equations and boundary conditions at successive orders of ε, the details of which now follow, as well as the form of the solutions at each order and details of how the coefficients in the solutions depend on the governing parameters.

At $O(\varepsilon)$, the governing equations (3.3) give, for $0 < x < 1$,

$$n_s\frac{\partial u_1}{\partial x} + \kappa n_1 = 0, \tag{A.1a}$$

$$M(n_s)u_1 - 2n_s\frac{\partial^2 u_1}{\partial x^2} + \beta_1\frac{\partial n_1}{\partial x} + \beta_2\frac{\partial c_1}{\partial x} = 0, \tag{A.1b}$$

$$\frac{\partial^2 c_1}{\partial x^2} + n_1 - \alpha_0 c_1 = 0, \tag{A.1c}$$

and the boundary conditions (3.4) at $O(\varepsilon)$ are

$$u_1 = 0, \quad \frac{\partial c_1}{\partial x} = 0 \quad \text{at} \quad x = 0, 1. \tag{A.2}$$

Considering perturbations of wavenumber π, equations (A.1) subject to (A.2) give

$$n_1 = A(T)\cos\pi x, \quad u_1 = -\frac{\kappa}{n_s\pi}A(T)\sin\pi x, \quad c_1 = \frac{A(T)}{\alpha_0 + \pi^2}\cos\pi x, \tag{A.3}$$

where $A(T)$ is an amplitude which will be determined at $O(\varepsilon^3)$.

At $O(\varepsilon^2)$ the governing equations are

$$n_s\frac{\partial u_2}{\partial x}+\kappa n_2 = -\frac{\partial}{\partial x}(n_1u_1), \tag{A.4a}$$

$$M(n_s)u_2-2n_s\frac{\partial^2u_2}{\partial x^2}+\beta_1\frac{\partial n_2}{\partial x}+\beta_2\frac{\partial c_2}{\partial x} = -M'(n_s)n_1u_1+2\frac{\partial}{\partial x}\left(n_1\frac{\partial u_1}{\partial x}\right) -\frac{\partial^2\Psi}{\partial c\partial n}\bigg|_{n_s,c_s}\frac{\partial}{\partial x}(n_1c_1)-\frac{\partial^2\Psi}{\partial c^2}\bigg|_{n_s,c_s}c_1\frac{\partial c_1}{\partial x}-\frac{\partial^2\Psi}{\partial n^2}\bigg|_{n_s,c_s}n_1\frac{\partial n_1}{\partial x}, \tag{A.4b}$$

$$\frac{\partial^2c_2}{\partial x^2}+n_2-\alpha_0c_2 = \frac{1}{(1-n_s)}\frac{\partial}{\partial x}\left(n_1\frac{\partial c_1}{\partial x}\right)-\alpha_1c_s+\frac{n_1(n_1-\alpha_0c_1)}{1-n_s}, \tag{A.4c}$$

which must be solved subject to

$$u_2=0,\quad \frac{\partial c_2}{\partial x}=0\quad\text{at}\quad x=0,1. \tag{A.5}$$

Equations (A.4) subject to (A.5) have solutions

$$n_2=N_2A^2\cos2\pi x,\quad u_2=U_2A^2\sin2\pi x,\quad c_2=C_{21}A^2\cos2\pi x+C_{22}A^2+C_{23}, \tag{A.6}$$

where N_2, U_2, C_{21}, C_{22} and C_{23} are constant coefficients. These coefficients are found by substituting (A.6) into (A.4), and have the following expressions

$$N_2 = \frac{1}{\Delta}\left[(4\pi^2+\alpha_0)\left(\Delta_1+\frac{\Delta_2}{n_s}\right)+\frac{2n_s\pi^4\beta_2}{(1-n_s)(\alpha_0+\pi^2)}\right], \tag{A.7a}$$

$$U_2 = -\frac{\kappa}{2n_s\pi}\left(N_2-\frac{1}{n_s}\right), \tag{A.7b}$$

$$C_{21} = \frac{1}{4\pi^2+\alpha_0}\left(N_2+\frac{\pi^2}{2(1-n_s)(\alpha_0+\pi^2)}\right), \tag{A.7c}$$

$$C_{22} = -\frac{\pi^2}{2\alpha_0(1-n_s)(\alpha_0+\pi^2)}, \tag{A.7d}$$

$$C_{23} = \frac{\alpha_1n_s}{\alpha_0^2}, \tag{A.7e}$$

where

$$\Delta = -4n_s\pi^2\beta_2+(4\pi^2+\alpha_0)(\Delta_2-4n_s\pi^2\beta_1), \tag{A.8a}$$

$$\Delta_1 = \kappa(M'(n_s)+4\pi^2)+\frac{2\pi^2n_s}{\alpha_0+\pi^2}\frac{\partial^2\Psi}{\partial n\partial c}\bigg|_{n_s,c_s}+\frac{\pi^2n_s}{(\alpha_0+\pi^2)^2}\frac{\partial^2\Psi}{\partial c^2}\bigg|_{n_s,c_s}+\pi^2n_s\frac{\partial^2\Psi}{\partial n^2}\bigg|_{n_s,c_s}, \tag{A.8b}$$

$$\Delta_2 = -\kappa(M(n_s)+8n_s\pi^2). \tag{A.8c}$$

At $O(\varepsilon^3)$ we have

$$n_s\frac{\partial u_3}{\partial x}+\kappa n_3=-\frac{\partial^2 n_1}{\partial T^2}-\frac{\partial}{\partial x}(n_1u_2+n_2u_1), \tag{A.9a}$$

$$\begin{aligned}M(n_s)u_3-2n_s\frac{\partial^2 u_3}{\partial x^2}+\beta_1\frac{\partial n_3}{\partial x}+\beta_2\frac{\partial c_3}{\partial x}&=-M'(n_s)n_1u_2-\left[n_2M'(n_s)+\frac{n_1^2}{2}M''(n_s)\right]u_1\\&+2\frac{\partial}{\partial x}\left(n_1\frac{\partial u_2}{\partial x}+n_2\frac{\partial u_1}{\partial x}\right)-\left.\frac{\partial^2\Psi}{\partial c\partial n}\right|_{n_s,c_s}\frac{\partial}{\partial x}(n_1c_2+n_2c_1)\\&-\left.\frac{\partial^2\Psi}{\partial c^2}\right|_{n_s,c_s}\frac{\partial}{\partial x}(c_1c_2)-\frac{c_1^2}{2}\left.\frac{\partial^3\Psi}{\partial c^3}\right|_{n_s,c_s}\frac{\partial c_1}{\partial x}-\frac{n_1^2}{2}\left.\frac{\partial^3\Psi}{\partial n^3}\right|_{n_s,c_s}\frac{\partial n_1}{\partial x}\\&-\frac{1}{2}\left.\frac{\partial^2\Psi}{\partial c^2\partial n}\right|_{n_s,c_s}\frac{\partial}{\partial x}(n_1c_1^2)-\frac{1}{2}\left.\frac{\partial^2\Psi}{\partial n^2\partial c}\right|_{n_s,c_s}\frac{\partial}{\partial x}(n_1^2c_1)-\left.\frac{\partial^2\Psi}{\partial n^2}\right|_{n_s,c_s}\frac{\partial}{\partial x}(n_1n_2),\end{aligned} \tag{A.9b}$$

$$\begin{aligned}\frac{\partial^2 c_3}{\partial x^2}+n_3-\alpha_0c_3=\frac{1}{(1-n_s)}&\left[\frac{\partial}{\partial x}\left(n_1\frac{\partial c_2}{\partial x}+n_2\frac{\partial c_1}{\partial x}\right)\right.\\&\left.+n_1(n_2-\alpha_0c_2)+n_2(n_1-\alpha_0c_1)-\alpha_1c_1(1-n_s)+\alpha_1n_1c_s\right].\end{aligned} \tag{A.9c}$$

B. Thin-film extensional flow model

We now present details of the weakly nonlinear analysis governed by equations (4.10)-(4.12) and (4.15) subject to boundary conditions (4.16a–c). The analysis proceeds along the same lines as presented in Appendix A. Below we present details of the governing equations and boundary conditions at successive orders of ε, as well as the form of the solutions at each order and expressions for the constant coefficients appearing in the solution.

At $O(\varepsilon)$ the governing equations are

$$n_sh_s\frac{\partial u_1}{\partial x}+h_s\kappa n_1 = 0, \tag{B.1a}$$

$$2n_sh_s\frac{\partial^2 u_1}{\partial x^2}+\Upsilon h_s\frac{\partial^3 h_1}{\partial x^3}-\Lambda u_1 = 0, \tag{B.1b}$$

$$h_s\frac{\partial u_1}{\partial x}+h_sK(n_s)\left(\beta_1\frac{\partial^2 n_1}{\partial x^2}+\beta_2\frac{\partial^2 c_1}{\partial x^2}\right) = 0, \tag{B.1c}$$

$$\frac{\partial^2 c_1}{\partial x^2}+n_1-\alpha_0c_1 = 0. \tag{B.1d}$$

Solving equations (B.1) subject to the $O(\varepsilon)$ boundary conditions

$$\frac{\partial n_1}{\partial x}=\frac{\partial h_1}{\partial x}=\frac{\partial c_1}{\partial x}=u_1=0, \quad \text{at} \quad x=0,1, \tag{B.2}$$

we find that

$$n_1=A(T)\cos\pi x, \quad u_1=\mathscr{U}A(T)\sin\pi x, \quad c_1=\mathscr{C}A(T)\cos\pi x, \quad h_1=\mathscr{H}A(T)\cos\pi x, \tag{B.3}$$

where $\mathscr{U}$, $\mathscr{C}$, and $\mathscr{H}$ have been introduced for notational convenience, and are given by

$$\mathscr{U}=-\frac{\kappa}{n_s\pi}, \quad \mathscr{C}\frac{1}{\alpha_0+\pi^2}, \quad \mathscr{H}=-\frac{\kappa}{\Upsilon h_sn_s\pi^4}(\Lambda+2h_sn_s\pi^2). \tag{B.4}$$

At $O(\varepsilon^2)$ the equations are

$$n_s h_s \frac{\partial u_2}{\partial x} + h_s \kappa n_2 = -n_s \frac{\partial}{\partial x}(h_1 u_1) - h_s \frac{\partial}{\partial x}(n_1 u_1) - \kappa h_1 n_1, \tag{B.5a}$$

$$2n_s h_s \frac{\partial^2 u_2}{\partial x^2} + \Upsilon h_s \frac{\partial^3 h_2}{\partial x^3} - \Lambda u_2 = -2\frac{\partial}{\partial x}\left((h_s n_1 + n_s h_1)\frac{\partial u_1}{\partial x} - n_s u_1 \frac{\partial h_1}{\partial x}\right) - \Upsilon h_1 \frac{\partial^3 h_1}{\partial x^3}, \tag{B.5b}$$

$$\begin{aligned} &h_s \frac{\partial u_2}{\partial x} + h_s K(n_s)\left(\beta_1 \frac{\partial^2 n_2}{\partial x^2} + \beta_2 \frac{\partial^2 c_2}{\partial x^2}\right) \\ &\quad = -\frac{\partial}{\partial x}\left[h_1 u_1 + h_s K(n_s)\left(\frac{\partial^2 \Psi}{\partial c \partial n}\bigg|_{n_s,c_s} \frac{\partial}{\partial x}(n_1 c_1) + \frac{\partial^2 \Psi}{\partial c^2}\bigg|_{n_s,c_s} c_1 \frac{\partial c_1}{\partial x} + \frac{\partial^2 \Psi}{\partial n^2}\bigg|_{n_s,c_s} n_1 \frac{\partial n_1}{\partial x}\right)\right. \\ &\qquad \left. + \big(h_1 K(n_s) + h_s n_1 K'(n_s)\big)\left(\beta_1 \frac{\partial n_2}{\partial x} + \beta_2 \frac{\partial c_2}{\partial x}\right)\right], \end{aligned} \tag{B.5c}$$

$$\begin{aligned} \frac{\partial^2 c_2}{\partial x^2} + n_2 - \alpha_0 c_2 = \frac{1}{h_s(1-n_s)}\Bigg[&-\frac{\partial}{\partial x}\left((h_1(1-n_s) - h_s n_1)\frac{\partial c_1}{\partial x}\right) \\ &-(n_1 - \alpha_0 c_1)(h_1(1-n_s) - n_1 h_s) - \alpha_1 c_s h_s (1-n_s)\Bigg], \end{aligned} \tag{B.5d}$$

subject to boundary conditions

$$\frac{\partial n_2}{\partial x} = \frac{\partial h_2}{\partial x} = \frac{\partial c_2}{\partial x} = u_2 = 0, \quad \text{at} \quad x = 0, 1. \tag{B.6}$$

The solutions are of the form

$$n_2 = N_{21} A^2 \cos 2\pi x + N_{22} A^2, \quad u_2 = U_2 A^2 \sin 2\pi x, \tag{B.7a}$$

$$h_2 = H_2 A^2 \cos 2\pi x, \quad c_2 = C_{21} A^2 \cos 2\pi x + C_{22} A^2 + C_{23}, \tag{B.7b}$$

where N_{21}, N_{22}, U_2, H_2, C_{21}, C_{22} and C_{23} are constants, as follows:

$$N_{21} = \frac{16h_s^2\pi^4\Upsilon}{\Delta_3}\left[(4\pi^2+\alpha_0)(-\mathbb{C}_1+n_s\mathbb{C}_3)-4n_s\pi^2K(n_s)\beta_2h_s\mathbb{C}_4\right], \tag{B.8a}$$

$$N_{22} = -\frac{\mathscr{H}}{2h_s}, \tag{B.8b}$$

$$U_2 = \frac{8h_s^2\pi^3\Upsilon}{\Delta_3}\left[-4K(n_s)\pi^2\mathbb{C}_1(\beta_2+4\pi^2\beta_1+\alpha_0\beta_1)\right.$$
$$\left.-\mathbb{C}_3\kappa(4\pi^2+\alpha_0)+4\mathbb{C}_4\beta_2K(n_s)\kappa\pi^2h_s\right], \tag{B.8c}$$

$$H_2 = \frac{1}{\Delta_3}\left[-4\pi^2K(n_s)n_sh_s\mathbb{C}_1(8\pi^2h_s+\Lambda)(\beta_2+\beta_1(4\pi^2+\alpha_0))+\frac{\Delta_3\mathbb{C}_2}{8\Upsilon\pi^3h_s}\right.$$
$$\left.-\kappa n_sh_s\mathbb{C}_3(8\pi^2h_s+\Lambda)(4\pi^2+\alpha_0)+4h_s^2n_s\pi^2\kappa K(n_s)\beta_2\mathbb{C}_4(8\pi^2h_s+\Lambda)\right], \tag{B.8d}$$

$$C_{21} = \frac{16h_s^2\pi^4\Upsilon}{\Delta_3}\left[-\mathbb{C}_1+n_2\mathbb{C}_3+h_s\kappa\mathbb{C}_4+4\mathbb{C}_4h_sn_s\pi^2\beta_1K(n_s)\right], \tag{B.8e}$$

$$C_{22} = \frac{1}{2\alpha_0h_s(1-n_s)}\left[-\alpha_0\mathscr{H}\mathscr{C}(1-n_s)-h_s(1-\alpha_0\mathscr{C})\right], \tag{B.8f}$$

$$C_{23} = \frac{n_s\alpha_1}{\alpha_0^2}. \tag{B.8g}$$

(B.8h)

where

$$\Delta_3 = -16\Upsilon\pi^4h_s^3\left[4n_s\pi^2\beta_2K(n_s)+(4\pi^2+\alpha_0)\kappa+4n_spi^2\beta_1K(n_s)(4\pi^2+\alpha_0)\right] \tag{B.9a}$$

$$\mathbb{C}_1 = -h_s\pi\mathscr{U}-n_s\pi\mathscr{U}\mathscr{H}-\frac{1}{2}\kappa\mathscr{H}, \tag{B.9b}$$

$$\mathbb{C}_2 = \frac{\pi^2}{2}\left(4\mathscr{U}h_s-\Upsilon\pi\mathscr{H}^2+\frac{\Lambda\mathscr{U}}{\pi^2}\right), \tag{B.9c}$$

$$\mathbb{C}_3 = -\pi\left[\mathscr{U}\mathscr{H}-2h_sK(n_s)\mathscr{C}\pi\left.\frac{\partial^2\Psi}{\partial n\partial c}\right|_{n_s,c_s}-h_sK(n_s)\mathscr{C}^2\pi\left.\frac{\partial^2\Psi}{\partial c^2}\right|_{n_s,c_s}-\mathscr{H}\pi K(n_s)\beta_1\right. \tag{B.9d}$$
$$\left.-\mathscr{H}\mathscr{C}\pi K(n_s)\beta_2-h_s\pi K'(n_s)\beta_1-h_s\pi K'(n_s)\beta_2\mathscr{C}-h_sK(n_s)\pi\left.\frac{\partial^2\Psi}{\partial n^2}\right|_{n_s,c_s}\right],$$

$$\mathbb{C}_4 = \frac{1}{2(1-n_s)h_s}\left(\mathscr{H}(1-n_s)-h_s\right)\left(2\pi^2\mathscr{C}-1+\alpha_0\mathscr{C}\right). \tag{B.9e}$$

Finally, the $O(\varepsilon^3)$ the governing equations are

$$n_sh_s\frac{\partial u_3}{\partial x}+h_s\kappa n_3 = -\frac{\partial}{\partial T}(h_sn_1+n_sh_1)-\frac{\partial}{\partial x}\left[(h_sn_1+n_sh_1)u_2+(n_sh_2+n_1h_1+h_sn_2)u_1\right]$$
$$-\kappa(h_1n_2+n_1h_2), \tag{B.10}$$

$$2n_s h_s \frac{\partial^2 u_3}{\partial x^2} + \Upsilon h_s \frac{\partial^3 h_3}{\partial x^3} - \Lambda u_3 = -\Upsilon h_1 \frac{\partial^3 h_2}{\partial x^3} - \Upsilon h_2 \frac{\partial^3 h_1}{\partial x^3} - 2\frac{\partial}{\partial x}\left[(h_1 n_s + n_1 h_s)\frac{\partial u_2}{\partial x}\right.$$
$$\left. + (h_2 n_s + n_1 h_1 + n_2 h_s)\frac{\partial u_1}{\partial x} - n_s\left(\frac{\partial h_1}{\partial T} + u_1\frac{\partial h_2}{\partial x} + u_2\frac{\partial h_1}{\partial x}\right) - n_1 u_1 \frac{\partial h_1}{\partial x}\right], \quad \text{(B.11)}$$

$$h_s \frac{\partial u_3}{\partial x} + h_s K(n_s)\left(\beta_1\frac{\partial^2 n_3}{\partial x^2} + \beta_2\frac{\partial^2 c_3}{\partial x^2}\right) = -\frac{\partial h_1}{\partial T} - \frac{\partial}{\partial x}(h_1 u_2 + h_2 u_1)$$
$$- \frac{\partial}{\partial x}\left[h_s K(n_s)\left(\left.\frac{\partial^2\Psi}{\partial c\partial n}\right|_{n_s,c_s}\frac{\partial}{\partial x}(n_2 c_1 + n_1 c_2) + \left.\frac{\partial^2\Psi}{\partial c^2}\right|_{n_s,c_s}\frac{\partial}{\partial x}(c_1 c_2) + \left.\frac{\partial^2\Psi}{\partial n^2}\right|_{n_s,c_s}\frac{\partial}{\partial x}(n_1 n_2)\right.\right.$$
$$\left.\left. + \frac{1}{2}\left(\left.\frac{\partial^2\Psi}{\partial c^2\partial n}\right|_{n_s,c_s}\frac{\partial}{\partial x}(n_1 c_1^2) + \left.\frac{\partial^3\Psi}{\partial c^3}\right|_{n_s,c_s} c_1^2\frac{\partial c_1}{\partial x} + \left.\frac{\partial^2\Psi}{\partial n^2\partial c}\right|_{n_s,c_s}\frac{\partial}{\partial x}(n_1^2 c_1) + \left.\frac{\partial^3\Psi}{\partial n^3}\right|_{n_s,c_s} n_1^2\frac{\partial n_1}{\partial x}\right)\right)\right.$$
$$+ \left(h_1 K(n_s) + h_s n_1 K'(n_s)\right)\left(\beta_1\frac{\partial n_2}{\partial x} + \left.\frac{\partial^2\Psi}{\partial c\partial n}\right|_{n_s,c_s}\frac{\partial}{\partial x}(c_1 n_1) + \beta_2\frac{\partial c_2}{\partial x} + \left.\frac{\partial^2\Psi}{\partial n^2}\right|_{n_s,c_s} n_1\frac{\partial n_1}{\partial x} + \left.\frac{\partial^2\Psi}{\partial c^2}\right|_{n_s,c_s} c_1\frac{\partial c_1}{\partial x}\right)$$
$$\left. + \left(\frac{K''(n_s)}{2}h_s n_1^2 + h_s K'(n_s)n_2 + K(n_s)h_2 + h_1 n_1 K'(n_s)\right)\left(\beta_1\frac{\partial n_2}{\partial x} + \beta_2\frac{\partial c_2}{\partial x}\right)\right], \quad \text{(B.12)}$$

$$\frac{\partial^2 c_3}{\partial x^2} + n_3 - \alpha_0 c_3 = \frac{1}{h_s(1-n_s)}\left[-\frac{\partial}{\partial x}\left((h_1(1-n_s) - h_s n_1)\frac{\partial c_2}{\partial x} + (h_2(1-n_s) - h_s n_2 - h_1 n_1)\frac{\partial c_1}{\partial x}\right)\right.$$
$$\left. - h_s(1-n_s)\alpha_1 c_1 - (n_2 - \alpha_0 c_2 + \alpha_1 c_s)(h_1(1-n_s) - n_1 h_s) - (h_2(1-n_s) - h_s n_2 - n_1 h_1)(n_1 - \alpha_0 c_1)\right]. \quad \text{(B.13)}$$

References

[1] A.R.A. Anderson and M. A. J. Chaplain. Continuous and discrete mathematical models of tumour-induced angiogenesis. *Bull. Math. Biol.*, 60:857–900, 1998.

[2] A. Aotani, M. Mimura, and T. Mollee. A model aided understanding of spot pattern formation in chemotactic *E. coli* colonies. *J. J. Ind. App. Maths.*, 27(1):5–22, 2010.

[3] C. J. W. Breward, H. M. Byrne, and C. E. Lewis. A multiphase model describing vascular tumour growth. *Bull. Math. Biol.*, 65 (4):609–640, 2003.

[4] H. M. Byrne and M. R. Owen. A new interpretation of the Keller-Segel model based on multiphase modelling. *J. Math. Biol*, 49(6):604–626, 2004.

[5] H. M. Byrne and L. Preziosi. Modelling solid tumour growth using the theory of mixtures. *Math. Med. Biol.*, 20:341–366, 2003.

[6] A. Q. Cai, K. A. Landman, and B. D. Hughes. Modelling directional guidance and motility regulation in cell migration. *Bull. Math. Biol.*, 68(1):25–52, 2006.

[7] N. G. Cogan, M. Donahue, and M. Whidden. Marginal stability and traveling fronts in two-phase mixtures. *Phys. Rev. E.*, 86:056204, 2012.

[8] D. A. Drew. Mathematical modelling of two-phase flow. *Ann. Rev. Fluid Mech.*, 15:261–291, 1983.

[9] L. Edelstein-Keshet. *Mathematical Models in Biology*. SIAM, 2005.

[10] L. Edelstein-Keshet and A. Spiros. Exploring the formation of Alzheimer's disease senile plaques in silico. *J. Theor. Biol.*, 216(3):301 – 326, 2002.

[11] R Eftimie, G de Vries, and MA Lewis. Weakly nonlinear analysis of a hyperbolic model for animal group formation. *J. Math. Biol.*, 59(1):37–74, 2009.

[12] J. E. F. Green. *Mathematical modelling of cell aggregation in liver tissue engineering*. PhD thesis, University of Nottingham, UK, 2006.

[13] J. E. F. Green, S. L. Waters, K. M. Shakesheff, and H. M. Byrne. A mathematical model of liver cell aggregation *in vitro*. *Bull. Math. Biol.*, 71:906–930, 2009.

[14] J. E. F. Green, S. L. Waters, J. P. Whiteley, L. Edelstein-Keshet, K. M. Shakesheff, and H. M. Byrne. Non-local models for the formation of hepatocyte - stellate cell aggregates. *J. Theor. Biol.*, 267(1):106–120, 2010.

[15] T. Hillen and K. J. Painter. A user's guide to pde models for chemotaxis. *J. Math. Biol.*, 58:183–217, 2009.

[16] N.L. Jeon, H. Baskaran, S.K.W Dertinger, G.M. Whitesides, L. Van De Water, and M. Tomer. Neutrophil chemotaxis in linear and complex grdaients of interleukin-8 formed in a microfabricated device. *Nat. Biotechnol.*, 20:826–830, 2002.

[17] P. Hansbo K. Eriksson, D. Estep and C. Johnson. *Computational Differential Equations*. Cambridge University Press, 1996.

[18] E. F. Keller and L. A. Segel. Initiation of slime mold aggregation viewed as an instability. *J. Theor. Biol.*, 26:399–415, 1970.

[19] E. F. Keller and L. A. Segel. Model for chemotaxis. *J. Theor. Biol.*, 30:225–234, 1971.

[20] L.S. Kimpton, J.P. Whiteley, S.L. Waters, J.R. King, and J.M. Oliver. Multiple travelling-wave solutions in a minimal model for cell motility. *Math. Med. Biol.*, 30:241–272, 2013.

[21] J. R. King and J. M. Oliver. Thin-film modelling of poroviscous free surface flows. *Euro. J. Appl. Math.*, 16:519–553, 2005.

[22] H. Knutsdottir, E. Palsson, and L. Edelstein-Keshet. Mathematical model of macrophage-facilitated breast cancer cells invasion. *J. Theor. Biol.*, 357:184–199, 2014.

[23] K. Landman, M. Simpson, J. Slater, and D. Newgreen. Diffusive and chemotactic cellular migration: Smooth and discontinuous traveling wave solutions. *SIAM J. Appl. Math.*, 65(4):1420–1442, 2005.

[24] G. Lemon, J. R. King, H. M. Byrne, O. E. Jensen, and K. M. Shakesheff. Mathematical modelling of engineered tissue growth using a multiphase porous flow mixture theory. *J. Math. Biol.*, 52:571–594, 2006.

[25] G. Lemon and J.R. King. Travelling-wave behaviour in a multiphase model of a population of cells in an artificial scaffold. *J. Math. Biol.*, 55(4):449–480, 2007.

[26] M. Luca, A. Chavez-Ross, L. Edelstein-Keshet, and A. Mogilner. Chemotactic signalling, microglia and Alzheimer's disease senile plaques: Is there a connection? *Bull. Math. Biol.*, 65:693–730, 2003.

[27] P.K. Maini and J. D. Murray. A nonlinear analysis of a mechanical model for biological pattern formation. *SIAM J. Appl. Math.*, 48(5):1064–1072, 1988.

[28] A. A. Neville, P. C. Matthews, and H. M. Byrne. Interactions between pattern formation and domain growth. *Bull. Math. Biol.*, 68(8):1975–2003, 2006.

[29] R.D. O'Dea, H.M. Byrne, and S.L. Waters. Continuum modelling of in vitro tissue engineering: a review. *Stud. Mechanobiol. Tissue Eng. Biomater.*, 10:229–266, 2013.

[30] R.D. O'Dea, J.M. Osborne, A.J. El-Haj, H.M. Byrne, and S.L. Waters. The interplay between tissue growth and scaffold degradation in engineered tissue constructs. *J. Math. Biol.*, 67:1199–1225, 2013.

[31] R.D. O'Dea, S.L. Waters, and H.M. Byrne. A multiphase model for tissue construct growth in a perfusion bioreactor. *Math. Med. Biol.*, 27(2):95–127, 2010.

[32] N.C. Pearson, S.L. Waters, J.M. Oliver, and Shipley. R.J. Multiphase modelling of the effect of fluid shear stress on cell yield and distribution in a hollow fibre membrane bioreactor. *Biomech. Mod. Mecanobiol.*, 2014.

[33] A.S. Perelson, P.K. Maini, J.D. Murray, J.M. Hyman, and G.F. Oster. Nonlinear pattern selection in a mechanical model for morphogenesis. *J. Math. Biol.*, 24(5):525–541, 1986.

[34] B.D. Sleeman and H.A. Levine. A system of reaction diffusion equations arising in the theory of reinforced random walks. *SIAM J. Appl. Math.*, 57:683–730, 1997.

[35] A. Stevens and H. G. Othmer. Aggregation, blowup and collapse: The ABC's of taxis in reinforced random walks. *SIAM J. Appl. Math.*, 57 (4):1044–1081, 1997.

[36] S. H. Strogatz. *Nonlinear dynamics and chaos*. Perseus, 1994.

[37] E. Süli and D. Mayers. *An Introduction to Numerical Analysis*. Cambridge University Press, 2003.

[38] B. L. Vaughan, R. E. Baker, D. Kay, and P. K. Maini. A modified Oster-Murray-Harris mechanical model of morphogenesis. *SIAM J. Appl. Math.*, 73(6):2124–2142, 2013.